CASL-U-2018-1507-000
ORNL/TM-2018/773

Development of Ultra-Fine Multi-Group Cross Section Library of the AMPX/SCALE Code Packages

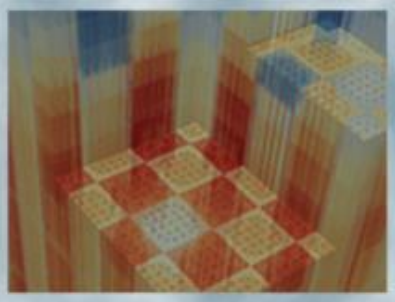

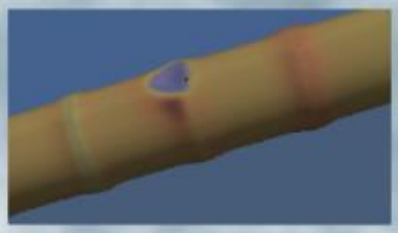

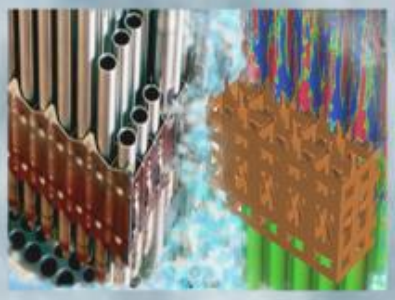

Byoung-kyu Jeon
Won Sik Yang
University of Michigan

Kang Seog Kim
Kevin Clarno
Oak Ridge National Laboratory

January 31, 2018

U.S. DEPARTMENT OF ENERGY | Nuclear Energy

DOCUMENT AVAILABILITY

Reports produced after January 1, 1996, are generally available free via US Department of Energy (DOE) SciTech Connect.

Website www.osti.gov

Reports produced before January 1, 1996, may be purchased by members of the public from the following source:

National Technical Information Service
5285 Port Royal Road
Springfield, VA 22161
Telephone 703-605-6000 (1-800-553-6847)
TDD 703-487-4639
Fax 703-605-6900
E-mail info@ntis.gov
Website http://classic.ntis.gov/

Reports are available to DOE employees, DOE contractors, Energy Technology Data Exchange representatives, and International Nuclear Information System representatives from the following source:

Office of Scientific and Technical Information
PO Box 62
Oak Ridge, TN 37831
Telephone 865-576-8401
Fax 865-576-5728
E-mail reports@osti.gov
Website http://www.osti.gov/contact.html

REVISION LOG

Revision	Date	Affected Pages	Revision Description
0	1/31/2018	All	Initial version

Export Controlled None

IP/Proprietary/NDA Controlled None

Sensitive Controlled None

Unlimited All Pages

Requested Distribution:

To: N/A

Copy: N/A

Reviewed by:

Date:

Reviewer:

EXECUTIVE SUMMARY

The Consortium for Advanced Simulation of Light Water Reactors Virtual Environment for Reactor Applications (VERA) neutronic simulator MPACT is being developed by Oak Ridge National Laboratory and the University of Michigan for various reactor applications. The MPACT and simplified MPACT 51- and 252-group cross section libraries have been developed for the MPACT neutron transport calculations by using the AMPX and Standardized Computer Analyses for Licensing Evaluations (SCALE) code packages developed at Oak Ridge National Laboratory. It has been noted that the conventional AMPX/SCALE procedure has limited applications for fast-spectrum systems such as boiling water reactor (BWR) fuels with very high void fractions and fast reactor fuels because of its poor accuracy in unresolved and fast energy regions. This lack of accuracy can introduce additional error sources to MPACT calculations, which is already limited by the Bondarenko approach for resolved resonance self-shielding calculation. To enhance the prediction accuracy of MPACT for fast-spectrum reactor analyses, the accuracy of the AMPX/SCALE code packages should be improved first.

The purpose of this study is to identify the major problems of the AMPX/SCALE procedure in generating fast-spectrum cross sections and to devise ways to improve the accuracy. For this, various benchmark problems including a typical pressurized water reactor fuel, BWR fuels with various void fractions, and several fast reactor fuels were analyzed using the AMPX 252-group libraries. Isotopic reaction rates were determined by SCALE multi-group (MG) calculations and compared with continuous energy (CE) Monte Carlo calculation results. This reaction rate analysis revealed three main contributors to the observed differences in reactivity and reaction rates: (1) the limitation of the Bondarenko approach in coarse energy group structure, (2) the normalization issue of probability tables, and (3) neglect of the self-shielding effect of resonance-like cross sections at high energy range such as (n,p) cross section of Cl^{35}. The first error source can be eliminated by an ultra-fine group (UFG) structure in which the broad scattering resonances of intermediate-weight nuclides can be represented accurately by a piecewise constant function. A UFG AMPX library was generated with modified probability tables and tested against various benchmark problems. The reactivity and reaction rates determined with the new UFG AMPX library agreed very well with respect to Monte Carlo Neutral Particle (MCNP) results.

To enhance the lattice calculation accuracy without significantly increasing the computational time, performing the UFG lattice calculation in two steps was proposed. In the first step, a UFG slowing-down calculation is performed for the corresponding homogenized composition, and UFG cross sections are collapsed into an intermediate group structure. In the second step, the lattice calculation is performed for the intermediate group level using the condensed group cross sections. A preliminary test showed that the condensed library reproduces the results obtained with the UFG cross section library. This result suggests that the proposed two-step lattice calculation approach is a promising option to enhance the applicability of the AMPX/SCALE system to fast system analysis.

CONTENTS

FIGURES

TABLES

ACRONYMS

2D	two-dimensional
ABTR	advanced burner test reactor
AMPX	resonance processing code; the name is no longer an acronym
BWR	boiling water reactor
CASL	Consortium for Advanced Simulation of Light Water Reactors
CE	continuous energy (as in cross sections)
CENTRM	Continuous ENergy Transport Module
ENDF	evaluated nuclear data file
ESSM	Embedded Self-Shielding Method
IR	intermediate resonance
MC^2-3	Multi-group cross section generation code for fast reactor analysis
MCNP	Monte Carlo Neutral Particle
MG	multi-group (as in cross sections)
MOC	method of characteristic
MPACT	radiation transport code; the name is no longer an acronym
MSR	molten salt reactor
NR	narrow resonance
ORNL	Oak Ridge National Laboratory
PW	pointwise
PWR	pressurized water reactor
RR	resolved resonances
SCALE	Standardized Computer Analyses for Licensing Evaluations
VERA	Virtual Environment for Reactor Applications
UFG	ultra-fine group (as in cross sections)
URR	unresolved resonance
XS	cross section

1 INTRODUCTION

The Consortium for Advanced Simulation of Light Water Reactors (CASL) [CAS15] Virtual Environment for Reactor Applications (VERA) [Tur16] neutronic simulator MPACT [Mpa13] is being developed by Oak Ridge National Laboratory (ORNL) and the University of Michigan. The MPACT and simplified MPACT 51- and 252-group cross section libraries [Kim17] have been generated for the MPACT neutron transport calculations using the AMPX [Wia16] and Standardized Computer Analyses for Licensing Evaluations (SCALE) [Sca16] code packages developed at ORNL. The self-shielded resonance cross section tables for fast, unresolved resonance (UR), and resolved resonance and thermal energy groups are generated by the narrow resonance (NR) approximation, analytic probability table method, and pointwise (PW) slowing-down calculations, respectively. The multi-group (MG) scattering matrices are processed by using typical PW neutron spectra for pressurized light water reactors (PWRs). The AMPX MG library can be developed by including these cross section processing procedures, which can be used for the conventional SCALE and MPACT transport calculations. Although the MPACT code adopts the subgroup method for the resonance self-shielding calculation, which is a Bondarenko approach requiring pre-calculated self-shielded resonance cross section tables, the SCALE procedure in the TRITON and CSAS sequences employs problem-dependent PW slowing-down calculations with Continuous ENergy Transport Module (CENTRM) to explicitly obtain self-shielded cross sections for resolved resonance energy groups. The CENTRM slowing-down calculations are also used to process the pre-calculated self-shielded resonance cross section tables for the MPACT subgroup method and the MG Embedded Self-Shielding Method (ESSM) [Wil12] used by the SCALE-Polaris code.

The conventional SCALE MG procedure with the AMPX 252 and 56-group libraries has been noted for its limited applications for fast-spectrum systems, such as boiling water reactor (BWR) fuels with very high void fractions and fast reactor fuels, because of the poor accuracy in unresolved and fast energy groups [Kim17]. This lack of accuracy can introduce additional error sources to MPACT calculations for conditions in which the absorption is sensitive to these energy ranges, which is already limited by the Bondarenko approach for resolved resonance self-shielding calculation. To identify the major issues for high energy groups, the AMPX 51- and 252-group libraries were tested for various benchmark problems including typical PWR fuels, BWR fuels with various void fractions, and several fast reactor fuels. Isotopic reaction rates were determined using SCALE multi-group (MG) calculations and compared with continuous energy (CE) Monte Carlo calculation results. This reaction rate analysis indicated that the observed discrepancies in fast-spectrum cross sections and scattering matrices mainly originated from the limitation of Bondarenko approach in a coarse energy group structure and a problem in probability tables. Additional minor issues were also identified in the cross sections in the AMPX MG library.

In fast-spectrum systems, the broad scattering resonances of intermediate-weight nuclides causes the strongly jagged structure of neutron spectrum. Thus, they cannot be treated as a constant background cross section for self-shielding of actinide resonance cross sections in the AMPX 51- and 252-group structures. To improve the applicability of the AMPX/SCALE code packages for fast-spectrum systems, it would be necessary to

adopt an ultra-fine group (UFG) structure so that the broad scattering resonances of intermediate-weight nuclides can be represented accurately by a piecewise constant function and to fix the identified problems.

The MC^2-3 [Lee11] code developed at Argonne National Laboratory is a typical MG cross section generation code for fast reactor applications. For given compositions, it solves the slowing-down equation in ultra-fine (~2,000) or hyper-fine (~400,000) group level. The UFG structure was selected to accurately represent the broad scattering resonances of intermediate-weight nuclides using a piecewise constant function. The actinide resonances are self-shielded using the NR approximation. The hyper-fine group (HFG) calculation may also be used to eliminate the errors in self-shielded UFG cross sections of actinides resulting from the NR approximation.

Using the equal lethargy interval of 1/120 in the UFG structure of MC^2-3, a new UFG AMPX library was generated in a 1,585-group structure and tested using various benchmark problems including typical PWR fuels, BWR fuels with various void fractions, and several fast reactor fuels. It was found that the new UFG AMPX cross section library noticeably enhances the accuracy of the AMPX/SCALE code packages for fast-spectrum applications. However, UFG lattice calculations were prohibitively expensive for practical design calculations. Thus, performing the UFG lattice calculation in two steps was proposed. In the first step, a UFG slowing-down calculation is performed for the corresponding homogenized composition, and UFG cross sections are collapsed into an intermediate group structure. In the second step, the lattice calculation is performed in the intermediate group level using the condensed group cross sections. A preliminary test of this two-step lattice calculation was performed using a simple benchmark problem.

The purpose of this report is to document the results of the benchmark analyses performed to identify the major problems of the current AMPX 252-group libraries and the performance of the new UFG AMPX library. The identified problems of the current libraries and the corresponding corrections are discussed. Detailed methodologies and procedures used for generating the UFG AMPX library are also included in this report. This remainder of this document addresses the following topics:

- Section 2 - Brief methodologies and procedures for the generation of AMPX and MPACT MG libraries. Generation of the AMPX MG libraries and verifications.
- Section 3 - Benchmark calculations and reaction rate analysis using the current 51- and 252-group AMPX libraries.
- Section 4 - Discussion of identified problems and corrections.
- Section 5 - Performance of a new AMPX 1,585-group library and the two-step lattice calculation.

2 LIBRARY GENERATION PROCEDURE AND VERIFICATION

The AMPX MG libraries are generated by using the AMPX-6 [Wia16] and SCALE [Sca16] code packages developed at ORNL. The methodologies and procedure to generate the AMPX MG libraries [Kim15] are briefly reviewed in this section.

2.1 LIBRARY GENERATION AND CROSS SECTION PROCESSING PROCEDURES

AMPX is a recently updated program that generates the AMPX MG and CE cross section libraries for SCALE and MPACT by processing evaluated nuclear data file (ENDF)/B libraries. The AMPX MG library includes resonance self-shielding factors called Bondarenko F-factors, principal cross sections and scattering matrices for all the ENDF/B nuclides, and fundamental control data. The AMPX code package processes the resonance self-shielding factors for resolved resonance groups by using the NR approximation and the probability table–based analytic formula coupled with the PW weighting functions for unresolved resonance groups. The smooth weighting function can be obtained by a combination of Maxwellian spectrum at thermal, 1/E spectrum at epithermal and fission spectrum at fast energy range, or typical PW PWR (or BWR) neutron spectra obtained by the CENTRM slowing-down calculation. In the resolved resonance and thermal ranges, the original resonance data based on the NR approximation are replaced by more accurate shielded data obtained from homogeneous and heterogeneous CENTRM calculations performed in the AMPX module IRFfactor. These data are used in improved Bondarenko approaches, such as the subgroup method and Embedded Self-Shielding Method employed in the CASL neutronics simulator MPACT and SCALE-Polaris, respectively. The resonance data are updated using the intermediate resonance (IR) approximation, which uses the IR parameters generated using the AMPX-LAMBDA code, and then the resonance data are updated by performing homogeneous or heterogeneous slowing-down calculations. Figure 2.1.1 [Kim17] illustrates a general sequence to generate the AMPX MG library.

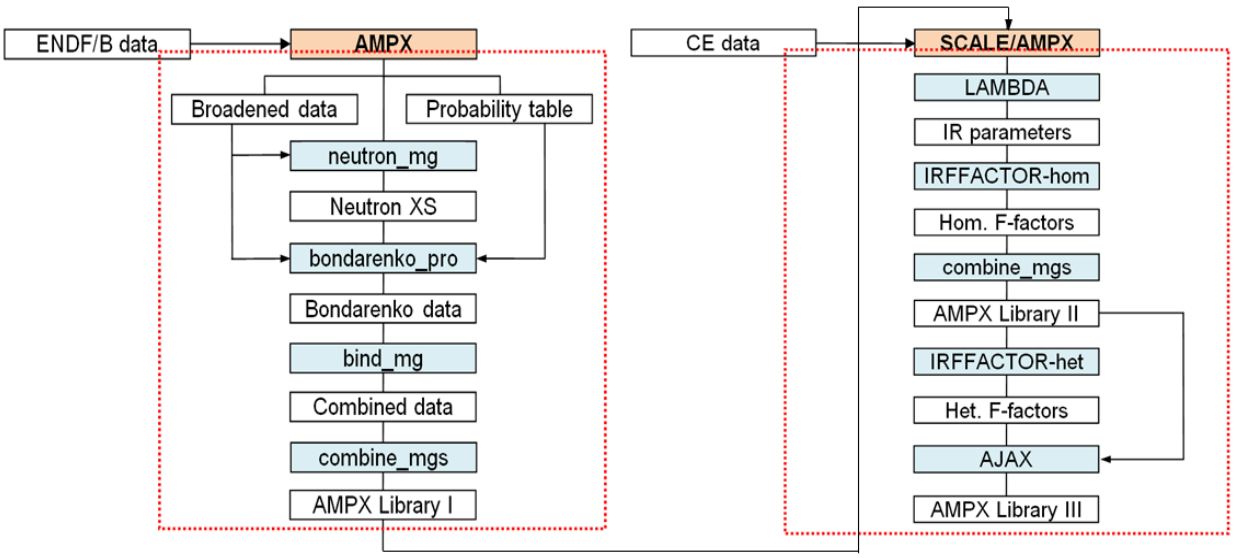

Figure 2.1.1. Flow chart of the AMPX procedure for generating MG libraries [Kim15].

Figure 2.1.2 provides the standard SCALE procedure to process problem-dependent MG cross sections and scattering matrices included in the AMPX MG working library by using several SCALE modules. BONAMI calculates self-shielded cross sections for all energy groups and nuclides based upon the conventional equivalence theory based Bondarenko approach. Then CENTRM performs the PW slowing-down calculations for resolved resonance and thermal energy ranges, which are coupled with the MG fixed source calculations for fast and very low energy groups. The MG cross sections for the PW energy range in CENTRM are obtained by flux weighting, and they replace the BONAMI-based cross sections to improve accuracy. This standard SCALE procedure has been used in this study.

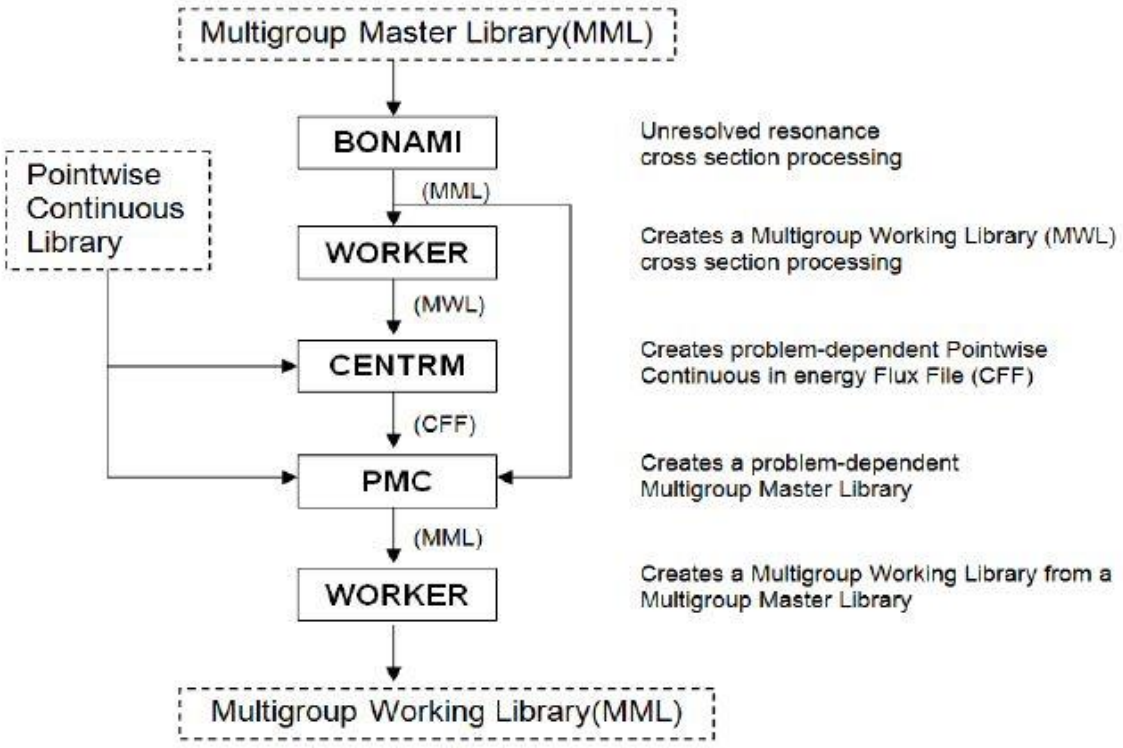

Figure 2.1.2. Sequence to generate the AMPX MG working library.

2.2 GENERATION OF THE AMPX 252- AND 1,585-GROUP LIBRARIES

Currently, SCALE 6.2 and the development version of SCALE include the AMPX 252- and 56-group libraries. To improve the accuracy of MPACT and simplified MPACT libraries for fast-spectrum system applications, the number of group structure of AMPX library was preliminarily increased from 252-groups to 1,585-groups by combining MC^2-3 [Lee11], UFG, and SCALE 252-group structures. Because the CEMTRM PW calculation is used to generate self-shielded cross sections in the resolved resonance region, the energy range from 0.1 keV to 14.2 MeV, which includes URR resonances for major isotopes, is divided into ultra-fine groups with an equal lethargy interval of 1/120. The remaining energy range is represented by 160 groups based on the current AMPX 252-

group structure. Table 2.2.1 illustrates the group structure of the 1,585-group library. Based on the near-term benchmark analysis need, the new 1,585-group library was prepared for 33 isotopes. Table 2.2.2 shows the list of isotopes and their descriptions.

Table 2.2.1. Group structure of the 1,585-group AMPX master library

Energy range (MeV)	No. groups	Self-shielding treatment	Group structure
10^{-11} ~ 10^{-9}	5	Bondarenko approach	AMPX 252-group
10^{-9} ~ 10^{-4}	151	CENTRM PW calculation	AMPX 252-group
10^{-4} ~ 14.2	1,425	Bondarenko approach	MC^2-3 2,082-group
14.2 ~ 20.0	4	Bondarenko approach	AMPX 252-group

Table 2.2.2. List of isotopes in the 1,585-group AMPX master library

No	Nuclides	Identifier	No	Nuclides	Identifier	No	Nuclides	Identifier
1	H^1	8001001	12	Zr^{90}	40090	23	U^{234}	92234
2	H in H_2O	1001	13	Zr^{91}	40091	24	U^{235}	92235
3	C-NAT	6000	14	Zr^{92}	40092	25	U^{236}	92236
4	graphite	3006000	15	Zr^{94}	40094	26	U^{238}	92238
5	O^{16}	8016	16	Mo^{92}	42092	27	Np^{237}	93237
6	Na^{23}	11023	17	Mo^{94}	42094	28	Pu^{239}	94239
7	Cl^{35}	17035	18	Mo^{95}	42095	29	Pu^{240}	94240
8	Cl^{37}	17037	19	Mo^{96}	42096	30	Pu^{241}	94241
9	Fe^{54}	26054	20	Mo^{97}	42097	31	Pu^{242}	94242
10	Fe^{56}	26056	21	Mo^{98}	42098	32	$Am^{242}m1$	1095242
11	Ni^{62}	28062	22	Mo^{100}	42100	33	Am^{243}	95243

The new AMPX 252- and 1,585-group master libraries were generated using the AMPX/SCALE code package with the procedure discussed in Section 2.1. Tables 2.2.3 and 2.2.4 provide details about the programs and data files used in the AMPX 252-group library generation. Because the resonance self-shielded cross sections for resolved resonance energy groups are prepared by the CENTRM PW slowing-down calculation, the IRFFACTOR-het step to generate the heterogeneous resonance data was skipped in this study. It was noted that the previous probability tables for the URR region had a normalization issue. Thus, a modified set of probability tables based on the ENDF/B-VII.1 data was recently prepared by ORNL and provided for this study. The 252- and 1,585-group AMPX libraries were regenerated using the new probability tables to estimate the accuracy improvement due to the modified probability tables.

Table 2.2.3. Programs to generate the AMPX MG library

Program	Location
[Jupiter.ornl.gov]	
AMPX6.3 beta1	/home/ykk/scale_dev0/build/first/INSTALL/bin/ampxrte
SCALE6.3 beta1	/home/ykk/scale_dev0/build/first/INSTALL/bin/scalerte
EXSITE	/scale/staging/6.3-rev23096/Ampx/exsite/bin/exsite

Table 2.2.4. Data files used in generating the AMPX MG library

Data File	Location
[Jupiter.ornl.gov]	
VII.1 Doppler broaden data	/home/dw8/libraries/endf/ENDF-B-VII.1/point/point/broaden_*
VII.1 Probability table	/home/dw8/libraries/endf7.1/ce/ptables/ptable_*
VII.1 Probability table_new	/home/hbq/ptabsWithNorm/ptables/
VII.1 Pointwise XS	/scale/scale_dev_data/cekenolib_7.1
VII.1 description file	/scale/scale_dev_data/ce_v7.1_endf
VII.1 xml file	/home/ykk/libraries/endf7.1/endf7.1.xml
VII.1 xml_config file	/home/ykk/libraries/endf7.1/endf7.1.xml_config
VII.1 weighting function	/home/ykk/libraries/wgtftn/200kev/casl_51g_50b00v_flux

3 BENCHMARK TESTS

To examine the performance of the AMPX MG libraries and the SCALE cross section processing procedure for various fuel cases, eight benchmark problems were developed including a typical PWR UO_2 fuel pin, five BWR UO_2 fuel pins with various void fractions, a simplified advanced burner test reactor (ABTR) fuel pin, and a homogenized molten salt reactor (MSR) fuel. Table 3.0.1 provides the brief description of benchmark problems. More detailed information can be found in Reference [Aki02] for the PWR and BWR problems, in Reference [Cha06] for ABTR, and in Reference [Tau80] for MSR. All the benchmark problems were simulated using a square pin cell geometry of MG-KENO. Each MG-KENO simulation was performed with 150 active cycles and 100,000 histories per cycle. Using the new 252- and 1,585-group AMPX master libraries, the MG cross sections were prepared as described in Figure 2.1.2. As discussed in Section 2.1, the self-shielded cross sections in the resolved resonance, and thermal regions were regenerated using the 2D method of characteristic (MOC) option of CENTRM except for MSR, which used the infinite homogeneous medium option. The isotopic compositions of the ABTR and MSR fuels are shown in Table 3.0.2.

Table 3.0.1 Benchmark problems

Fuel	Case	^{235}U w/o	Temperature (K)			Void (%)
			Fuel	Clad	Moderator	
PWR	A1	6.5	900	600	600	0
BWR	B1		900	600	600	40[a]
	B2		900	600	600	70[a]
	B3		900	600	600	90[a]
	B4		900	600	600	90[b]
	B5		900	600	600	99[b]
ABTR	C1	—	300	300	300	—
MSR	D1	—	300	300	300	—

[a] Assembly averaged void fraction by averaging in-channel moderator, and moderator in assembly gap, and water hole whose void fraction is zero.

[b] Cell-averaged void fraction.

Table 3.0.2 Isotopic composition for fast reactor problems C1 and D1

ABTR			Homogenized MSR	
Region	Nuclide	Number density	Nuclide	Number density
Fuel	92235	3.2247E-05	92235	3.1000E-05
	92238	2.0222E-02	92238	4.2750E-03
	94239	3.4991E-03	94239	4.0400E-04
	94240	3.7398E-04	94240	5.4000E-05
	40090	3.7526E-03	94241	2.7000E-05
Bond	11023	2.2272E-02	94242	5.4000E-05
Cladding	26054	4.0824E-03	11023	5.3830E-03
	26056	6.4085E-02	17035	1.5010E-02
Coolant	11023	2.2272E-02	17037	4.8332E-03

3.1 LWR BENCHMARK TESTS

Benchmark calculations were performed using the SCALE MG-KENO module with the ENDF/B-VII.1 AMPX 51- and 252-group libraries for benchmark cases A1 and B1–B5. The AMPX 51-group library was generated when the MPACT 51-group library was developed. The reference solutions were obtained by performing CE Monte Carlo Neutral Particle (MCNP) calculations with 1,000 active cycles and 100,000 histories per cycle to yield relative errors of reaction rates less than 0.3%. The BWR benchmark problems B1–B5 with different void fractions (40%–99%) show a wide range of neutron spectra ranging from thermal to fast. Figure 3.1.1 shows a comparison of neutron spectra for cases A1 and B1–B5. Note the asymptotic 1/E spectrum is not attained in the highly voided cases B4 and B5.

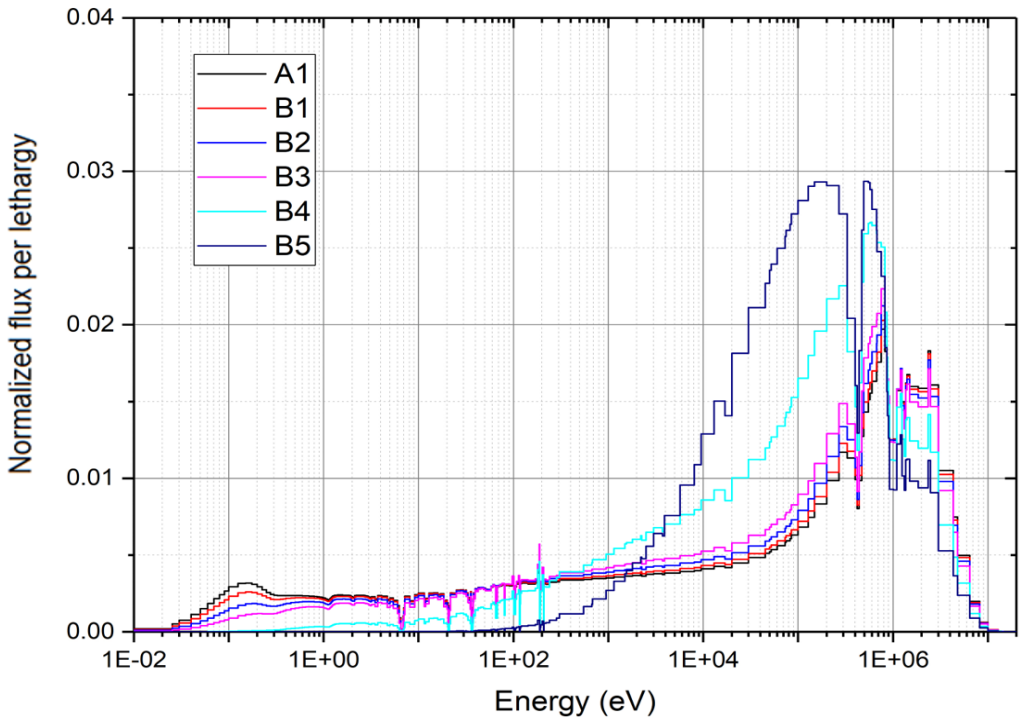

Figure 3.1.1. 252-group fluxes in fuel for UO_2 problems with various void fractions.

Tables 3.1.1 and 3.1.2 compare eigenvalues between the MG-KENO and MCNP results obtained with the 51- and 252-group AMPX libraries. The maximum eigenvalue differences between the MCNP6 and MG-KENO results are 2,710 and 654 pcm for the AMPX 51- and 252-group libraries, respectively. The 51-group results are much worse than the 252-group results for all cases. This indicates that the 51-group structure is not properly optimized to minimize the impact of angle-dependent total cross sections on energy group collapsing. SCALE's energy group condensation procedure approximately treats the angle-dependent total cross sections. However, the large eigenvalue error in the 252-group result for the BWR problem B5 suggests there are other error sources that need to be investigated.

Table 3.1.1 Eigenvalues of MG-KENO and MCNP6 for UO_2 pin cell problems

Fuel	Case	Void fraction (%)	Multiplication factor (k_{inf})				
			MCNP	MG-KENO			
				252-group	Δk (pcm)	51-group	Δk (pcm)
PWR	A1	0	1.43582 (6)	1.43436 (9)	−146 (10)	1.43212 (16)	−370 (17)
BWR	B1	40	1.39488 (6)	1.39337 (13)	−151 (14)	1.39166 (13)	−322 (14)
	B2	70	1.32518 (6)	1.32395 (16)	−123 (18)	1.32275 (19)	−243 (20)
	B3	90	1.24258 (6)	1.24159 (18)	−99 (19)	1.24095 (13)	−163 (17)
	B4	90	1.00980 (6)	1.01145 (12)	165 (13)	1.01887 (10)	907 (12)
	B5	99	0.91266 (4)	0.91920 (10)	654 (11)	0.93977 (9)	2,710 (11)

Figure 3.1.2 compares the 252-group neutron spectra of the BWR problem B5 obtained with MG-KENO and MCNP calculations. For this highly voided problem, the MG-KENO and MCNP flux spectra show non-negligible differences. Flux errors up to ~3.5% can be seen in the groups from 10 keV to 100 keV, which includes the URR ranges of heavy isotopes and most of wide resonances of zirconium isotopes. Furthermore, the k_∞ differences of the BWR problems B1–B5 with different void fractions do not show a clear trend. This also suggests that there may be other sources for the observed reactivity differences. Therefore, more detailed reaction rate analysis needs to be performed to assess the SCALE procedure to generate the 252-group cross sections for transport calculations.

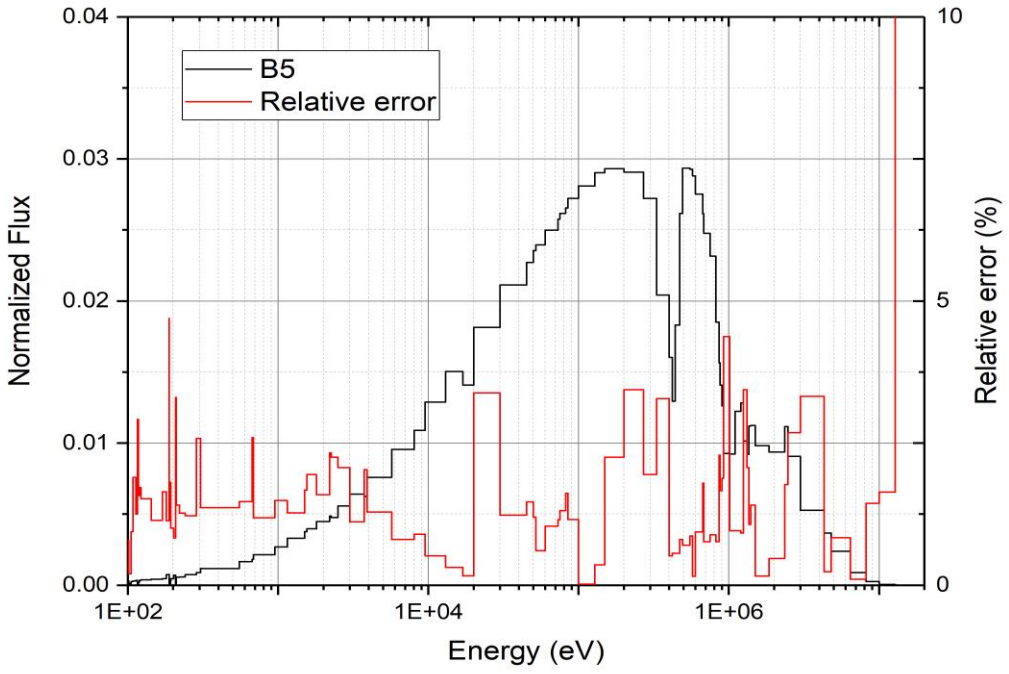

Figure 3.1.2. Comparison of 252-group fluxes obtained from MG-KENO and MCNP for 99% void BWR.

3.2 FAST REACTOR BENCHMARK TESTS

The SCALE procedure with the ENDF/B-VII.1 AMPX 51- and 252-group libraries have been assessed for the fast reactor fuels including a simplified ABTR fuel pin (case C1) and a homogeneous MSR fuel (case D1). Figure 3.2.1 shows the normalized neutron spectra per lethargy for cases C1 and D1. Again, the asymptotic 1/E spectrum is not attained in these fast reactor problems. Table 3.2.1 compares the multiplication factors of the MG-KENO and MCNP calculations and shows that both AMPX libraries yield significant reactivity differences. Even the 252-group library resulted in eigenvalue differences of 341 and 536 pcm for ABTR and MSR, respectively. The relative deviation of MG-KENO flux spectrum from MCNP flux is also shown in Figure 3.2.2. Maximum flux errors up to 13% can be seen in the groups from 10 keV to 100 keV. These results indicate that the current SCALE procedure with the AMPX MG library may not be applicable to the analysis of the fast-spectrum problems such as highly voided BWR problems and fast reactor problems.

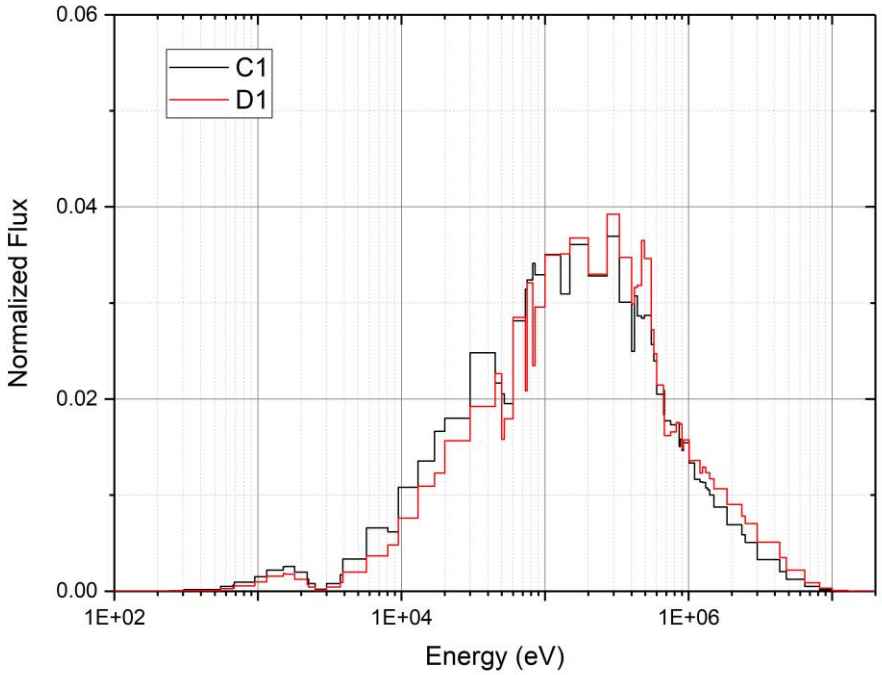

Figure 3.2.1. 252-group fluxes in fuel for the ABTR and MSR problems.

Table 3.2.1. Eigenvalues of MG-KENO and MCNP6 for ABTR and MSR pin cell problems

Fuel	Case	Multiplication factor (k_{inf})				
		MCNP	MG-KENO			
			252-group	Δk (pcm)	51-group	Δk (pcm)
ABTR	C1	1.60150 (4)	1.60491 (12)	341 (13)	1.60918 (11)	768 (11)
MSR	D1	1.13927 (1)	1.14463 (7)	536 (7)	1.16489 (8)	2,561 (8)

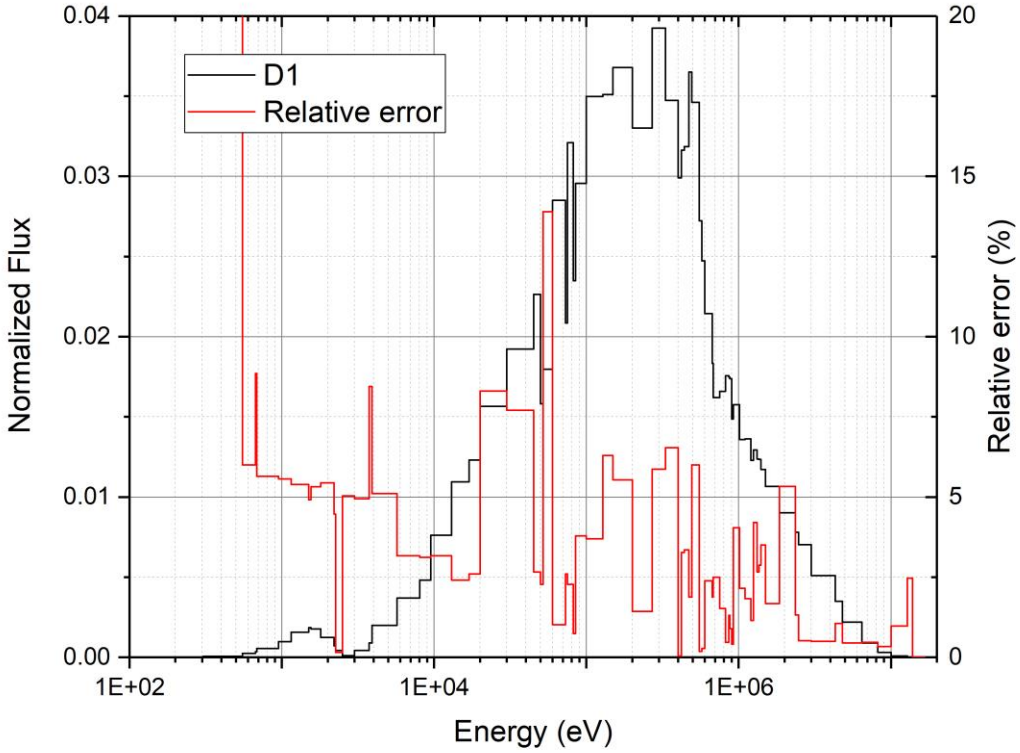

Figure 3.2.2. Comparison of 252-group fluxes in fuel obtained from MG-KENO and MCNP for the MSR problem.

3.3 REACTION RATE ANALYSIS

The benchmark results in Sections 3.1 and 3.2 show that the MG-KENO multiplication factors obtained with the AMPX 252-group library are generally consistent with the MCNP results, except for the highly voided BWR problem B5 and MSR problem D1. However, these results might be due to error cancellations, so more detailed analysis is required to quantitatively evaluate the quality of the MG cross sections. To identify the main error sources and the degree of error cancellation of the observed eigenvalue difference between MG-KENO and MCNP results, detailed reaction rate analyses were performed. The reaction rate difference between MG-KENO and MCNP and its contribution to the reactivity difference were estimated for each nuclide and each energy group following this process:

a. Perform the CE MCNP calculation and tally the MG scalar fluxes, isotopic capture and fission reaction rates, and average the number of neutrons released per fission ($\bar{\upsilon}$) in addition to eigenvalue.
b. Perform the standard SCALE MG-KENO calculation to obtain the parameters in step a.
c. Calculate the contribution to the reactivity difference of the reaction rate difference (i.e., cross section and flux errors) for each nuclide, reaction type, and energy group using the following formulas:

$$\Delta\rho^{k'}_{c,g',i'} = \frac{N^{k'}_{i'}(\sigma^{k'}_{c,g',i'}\phi_{g',i'} - \hat{\sigma}^{k'}_{c,g',i'}\hat{\phi}_{g',i'})V_{i'}}{\sum_i\sum_k\sum_g N^k_i \upsilon^k_{g,i}\sigma^k_{fis,g,i}\phi_{g,i}V_i}, \quad (3.3.1)$$

and

$$\Delta\rho^{k'}_{fis,g',i'} = \frac{1}{k_\infty} - \frac{\sum_i\sum_k\sum_g N^k_i(\sigma^k_{a,g,i} - \sigma^k_{n,2n,g,i} - 2\sigma^k_{n,3n,g,i})\phi_{g,i}V_i}{\sum_i\sum_k\sum_g N^k_i \upsilon^k_{g,i}\sigma^k_{fis,g,i}\phi_{g,i}V_i - N^{k'}_{i'}\upsilon^{k'}_{g',i'}(\sigma^{k'}_{fis,g',i'}\phi_{g',i'} - \hat{\sigma}^{k'}_{fis,g',i'}\hat{\phi}_{g',i'})V_{i'}}$$
$$+ \frac{N^{k'}_{i'}(\sigma^{k'}_{fis,g',i'}\phi_{g',i'} - \hat{\sigma}^{k'}_{fis,g',i'}\hat{\phi}_{g',i'})V_{i'}}{\sum_i\sum_k\sum_g N^k_i \upsilon^k_{g,i}\sigma^k_{fis,g,i}\phi_{g,i}V_i - N^{k'}_{i'}\upsilon^{k'}_{g',i'}(\sigma^{k'}_{fis,g',i'}\phi_{g',i'} - \hat{\sigma}^{k'}_{fis,g',i'}\hat{\phi}_{g',i'})V_{i'}}, \quad (3.3.2)$$

where $\Delta\rho^{k'}_{x',g',i'}$ is the reactivity differences due to the difference in the fission ($x = fis$) or capture ($x = c$) reaction rate of nuclide k' at group g' and region i'. N^k_i and V_i are the atomic number density of nuclide k and volume at region i, respectively. A quantity with caret (^) symbol indicates the cross section or flux from MG-KENO, whereas the other quantities are from MCNP. The multiplication factor (k_∞) in Eq. (3.3.2) can be estimated by using the following equation:

$$k_\infty = \frac{\sum_i\sum_k\sum_g N^k_i \upsilon^k_{g,i}\sigma^k_{fis,g,i}\phi_{g,i}V_i}{\sum_i\sum_k\sum_g N^k_i(\sigma^k_{a,g,i} - \sigma^k_{n,2n,g,i} - 2\sigma^k_{n,3n,g,i})\phi_{g,i}V_i}. \quad (3.3.3)$$

d. The direct effects of cross section errors (i.e., without considering the flux errors resulting from cross section errors) were also investigated using the reference MCNP flux in Eqs. (3.3.1) and (3.3.2) as

$$\Delta\rho^{k'}_{c,g',i'} = \frac{N^{k'}_{i'}(\sigma^{k'}_{c,g',i'}\phi_{g',i'} - \hat{\sigma}^{k'}_{c,g',i'}\hat{\phi}_{g',i'})V_{i'}}{\sum_i\sum_k\sum_g N^k_i \upsilon^k_{g,i}\sigma^k_{fis,g,i}\phi_{g,i}V_i}, \quad (3.3.4)$$

$$\Delta\rho^{k'}_{fis,g',i'} = \frac{1}{k_\infty} - \frac{\sum_i\sum_k\sum_g N^k_i(\sigma^k_{a,g,i} - \sigma^k_{n,2n,g,i} - 2\sigma^k_{n,3n,g,i})\phi_{g,i}V_i}{\sum_i\sum_k\sum_g N^k_i \upsilon^k_{g,i}\sigma^k_{fis,g,i}\phi_{g,i}V_i - N^{k'}_{i'}\upsilon^{k'}_{g',i'}(\sigma^{k'}_{fis,g',i'}\phi_{g',i'} - \hat{\sigma}^{k'}_{fis,g',i'}\phi_{g',i'})V_{i'}}$$
$$+ \frac{N^{k'}_{i'}\upsilon^{k'}_{g',i'}(\sigma^{k'}_{fis,g',i'}\phi_{g',i'} - \hat{\sigma}^{k'}_{fis,g',i'}\phi_{g',i'})V_{i'}}{\sum_i\sum_k\sum_g N^k_i \upsilon^k_{g,i}\sigma^k_{fis,g,i}\phi_{g,i}V_i - N^{k'}_{i'}\upsilon^{k'}_{g',i'}(\sigma^{k'}_{fis,g',i'}\phi_{g',i'} - \hat{\sigma}^{k'}_{fis,g',i'}\phi_{g',i'})V_{i'}}. \quad (3.3.5)$$

Tables 3.3.1 and 3.3.2 summarize the reaction rate analysis results obtained with Eqs. (3.3.1) and (3.3.2) by considering both cross section and flux differences. For the highly voided BWR problems B4 and B5, the impacts of Zr^{90} and O^{16} cross sections on reactivity are not negligible, so they are included in the reaction rate analysis. The values in the column “Code” represent the reactivity difference and its standard deviation

determined from the eigenvalue results of MG-KENO and MCNP. The other reactivity differences or changes are described in the Table 3.3.1 notes. The reactivity differences determined from two eigenvalues calculated using the tallied reaction rates with Eq. (3.3.3) are consistent with the simulated reactivities within two standard deviations. As shown in Table 3.3.1, the reactivity deviations of MG-KENO from MCNP are mostly due to the errors in U^{238} capture reaction rate. The effects on reactivity of the capture and fission reaction rates of U^{235} have opposite signs, which means they are partly canceled out, and except for B5, the net effect is significantly smaller than the capture reaction of U^{238}. This reaction rate analysis shows that the SCALE MG-KENO results are very consistent with the MCNP results for all cases except for the 99% void fraction in case B5. However, it is still possible that the good eigenvalue agreements are the result of error cancellation among energy groups. Therefore, the differences in group-wise reaction rates were also examined.

Table 3.3.1 Reaction rate analysis results for the PWR and BWR benchmark cases

Void fraction	Case	$\Delta\rho$ (pcm)		Nuclide	XS/Flux effect[b] (pcm)			XS effect[c] (pcm)		
		Code	RR[a]		RR_{cap}[d]	RR_{fis}[d]	SUM	RR_{cap}[d]	RR_{fis}[d]	SUM
0% (PWR)	A1	−71 (5)	−74	92235	18	−24	−73	−17	39	29
				92238	−69	-		8	−1	
40%	B1	−78 (7)	−82	92235	22	−40	−82	−18	42	24
				92238	−64	-		1	−1	
70%	B2	−70 (10)	−80	92235	20	−36	−80	−23	52	23
				92238	−61	−4		−5	−1	
90%	B3	−64 (12)	−57	92235	16	−12	−55	−29	70	19
				92238	−56	−3		−21	−1	
90%	B4	162 (13)	166	92235	13	11	167	−64	222	130
				92238	127	13		−34	1	
				8016	−6	—		−4	—	
				40090	9	—		9	—	
99%	B5	780 (13)	773	92235	−20	205	779	−106	480	479
				92238	543	32		81	3	
				8016	−9	—		−5	—	
				40090	29	—		26	—	

[a] Reactivity difference determined from two eigenvalues deduced from reaction rates with Eq. (3.3.3).

[b] Reactivity changes due to the cross section and fluxes differences obtained with Eqs. (3.3.1) and (3.3.2).

[c] Reactivity changes due to the cross section difference obtained with Eqs. (3.3.4) and (3.3.5).

[d] $RR_{cap} = \sum_g \Delta\rho^k_{c,g}$, $RR_{fis} = \sum_g \Delta\rho^k_{fis,g}$

Table 3.3.2 shows that in the fast reactors ABTR and MSR, there are more error cancellations among different reaction rates, especially between the capture and fission reactions of U^{238}, Pu^{239}, and Pu^{241}. In addition, Cl^{35} is a dominant negative contributor to the reactivity difference of the MSR problem. For Cl^{35}, the absorption reaction rate was

used instead of the capture reaction rate because Cl^{35} has a non-negligible (n,p) cross section at high energy groups. In the ABTR and MSR problems, the reactivity differences due to the differences in cross section and flux differ greatly from the reactivity differences due to the cross section difference only. This indicates that the scattering matrices as well as principal cross sections are error sources of reactivity for fast reactor problems because the flux spectrum differences are primarily caused by the differences in scattering matrices.

Table 3.3.2 Reaction rate analysis results for the ABTR and MSR cases

Fuel	Case	$\Delta\rho$ [pcm]		Nuclide	XS/Flux effect [pcm]			XS effect [pcm]		
		Code	RR		RR_{cap}	RR_{fis}	SUM	RR_{cap}	RR_{fis}	SUM
ABTR	C1	133 (5)	135	92235	−1	1	135	−2	2	139
				92238	5	28		33	10	
				94239	−32	142		−131	248	
				94240	−4	5		-5	3	
				40090	9	—		9	—	
				11023	−12	—		−17	—	
				26056	−1	—		−1	—	
				26054	−6	—		−11	—	
MSR	D1	411 (5)	409	92235	4	-6	409	−5	15	−129
				92238	485	43		40	10	
				94239	125	86		—	244	
				94240	11	5		−4	3	
				94241	18	53		12	85	
				94242	4	4		−10	1	
				11023	4	0		−4	—	
				17035	−426	0		−517	—	

To investigate the group-wise contributions to the observed differences in reactivity and reaction rates, the MG-KENO and MCNP results were examined in more detail. First, the 252-group capture and fission cross sections of MG-KENO were compared with the corresponding tallied cross sections of MCNP for major nuclides. Then the direct effects on the reactivity error of the 252-group MG-KENO cross section errors were examined without considering the flux errors resulting from the MG-KENO cross section errors. The contribution to the reactivity difference of the MG-KENO reaction rate error that includes the flux error due to the cross section errors was also examined for each nuclide and each energy group.

Figure 3.3.1 compares the relative deviation of U^{235} capture cross sections of MG-KENO from MCNP tallies for the PWR and BWR benchmark cases A1, B4, and B5. Figure 3.3.2 compares the direct effects of U^{235} capture cross section errors on the reactivity error, and Figure 3.3.3 compares the reactivity error caused by the reaction rate error of U^{235} capture. Figures 3.3.4–3.3.6 show these three comparisons for the U^{235} fission reaction. Similar comparisons are presented in Figures 3.3.7–3.3.12 for U^{238} capture and fission reactions, and in Figures 3.3.13 and 3.3.14 for Zr^{90} capture reaction.

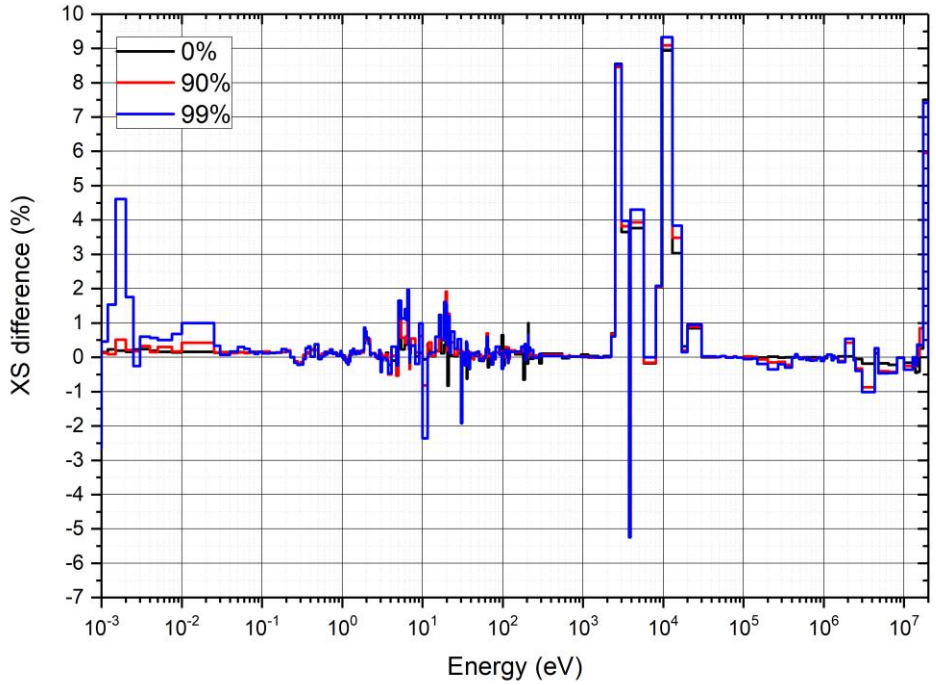

Figure 3.3.1. Comparison of U^{235} caption cross section differences between MG-KENO and MCNP for UO_2 fuel pin problems with various void fractions.

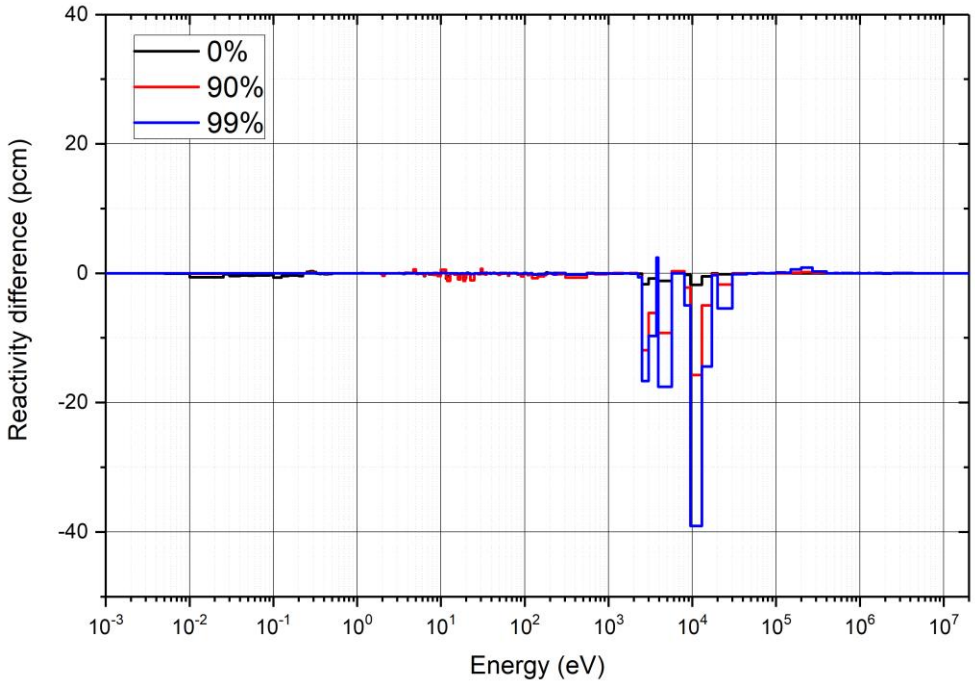

Figure 3.3.2. Reactivity differences due to the U^{235} capture cross section differences for UO_2 fuel pin problems with various void fractions.

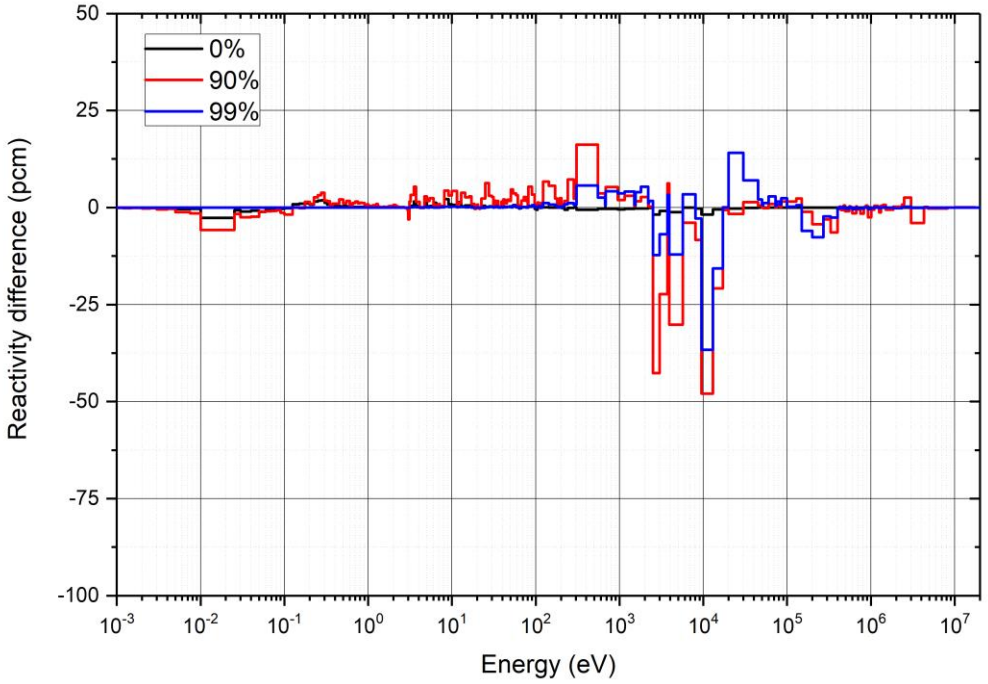

Figure 3.3.3. Reactivity differences due to the capture cross section and flux differences of U^{235} for UO_2 fuel pin problems with various void fractions.

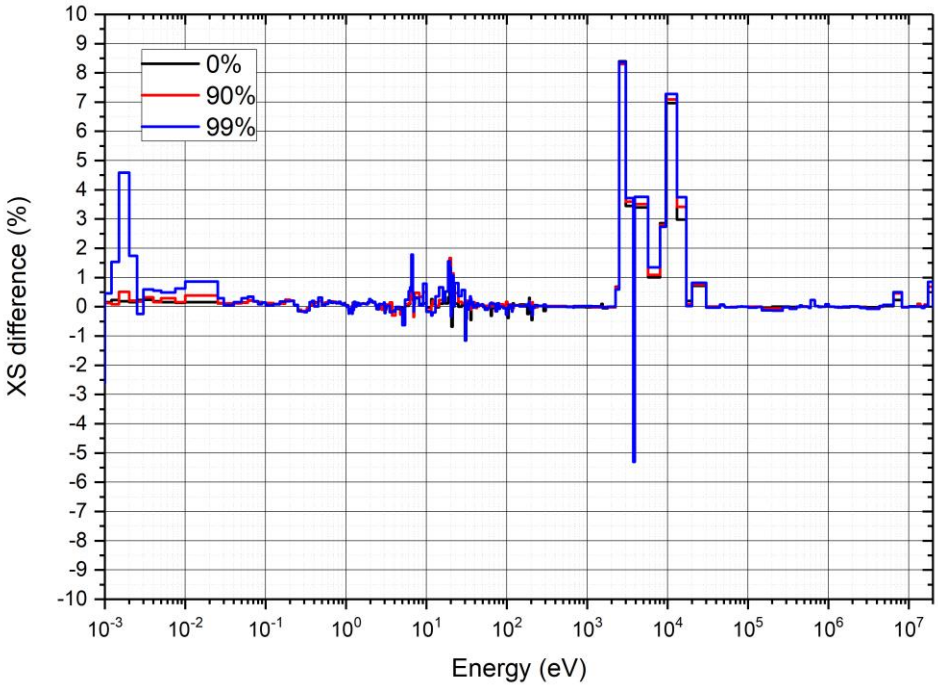

Figure 3.3.4. Comparison of U^{235} fission cross section differences between MG-KENO and MCNP for UO_2 fuel pin problems with various void fractions.

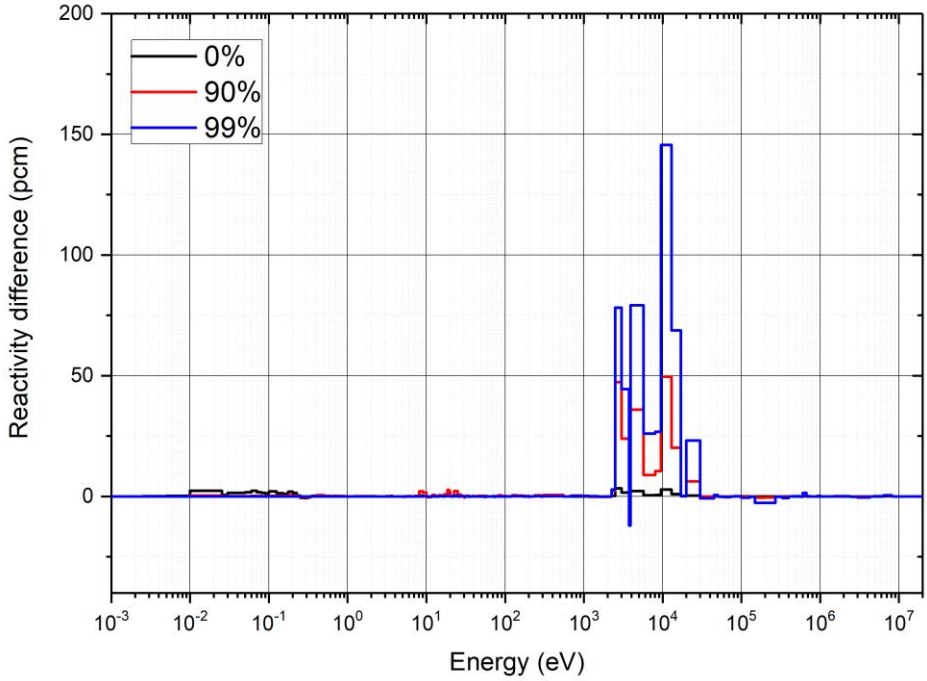

Figure 3.3.5. Reactivity differences due to the U^{235} fission cross section differences for UO_2 fuel pin problems with various void fractions.

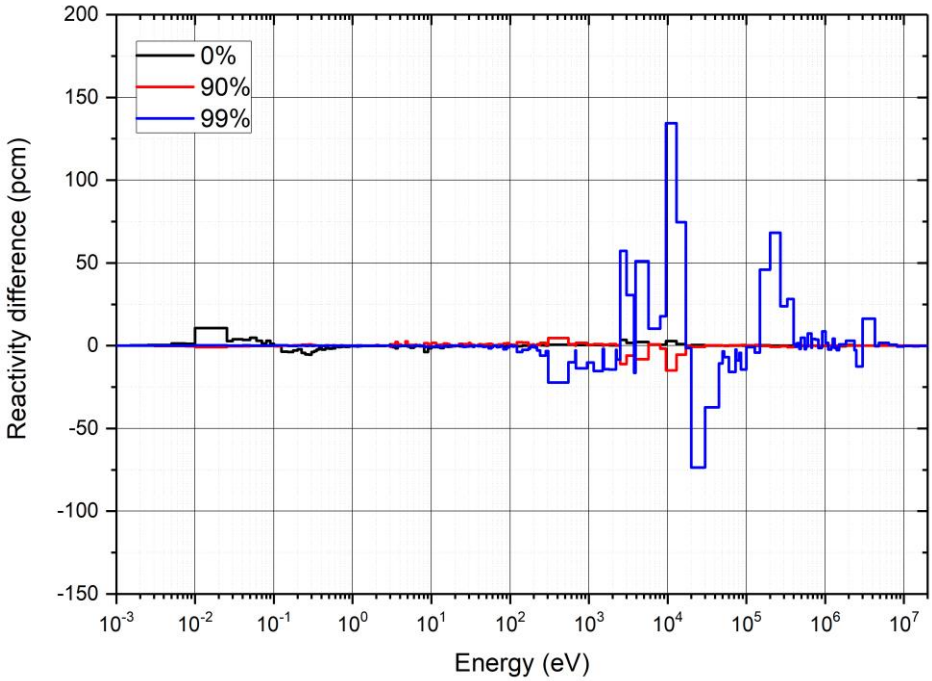

Figure 3.3.6. Reactivity differences due to the fission cross section and flux differences of U^{235} for UO_2 fuel pin problems with various void fractions.

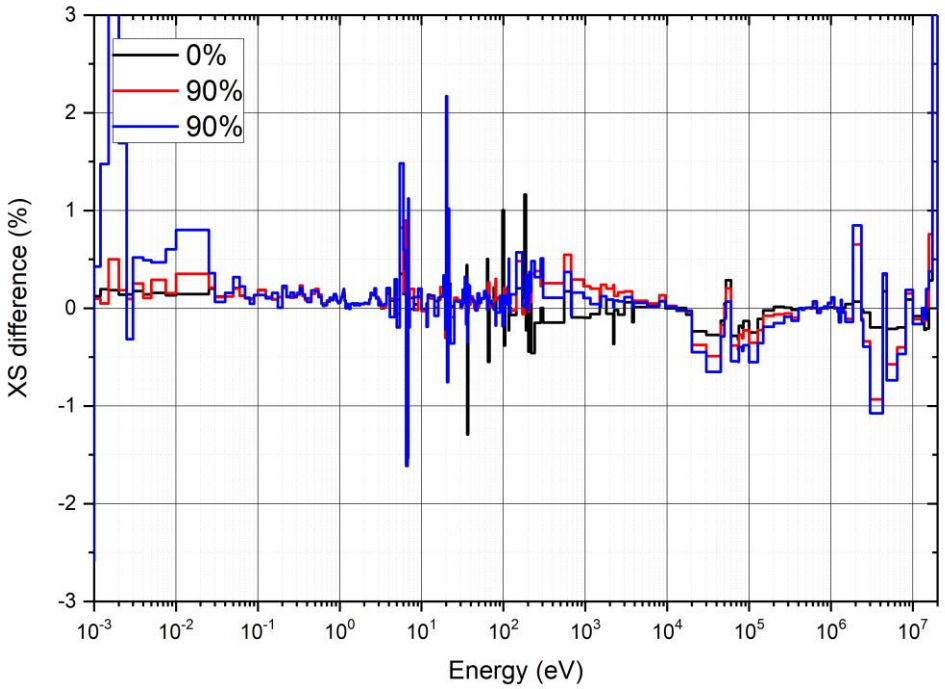

Figure 3.3.7. Comparison of U^{238} capture cross section differences in MG-KENO and MCNP for UO_2 fuel pin problems with various void fractions.

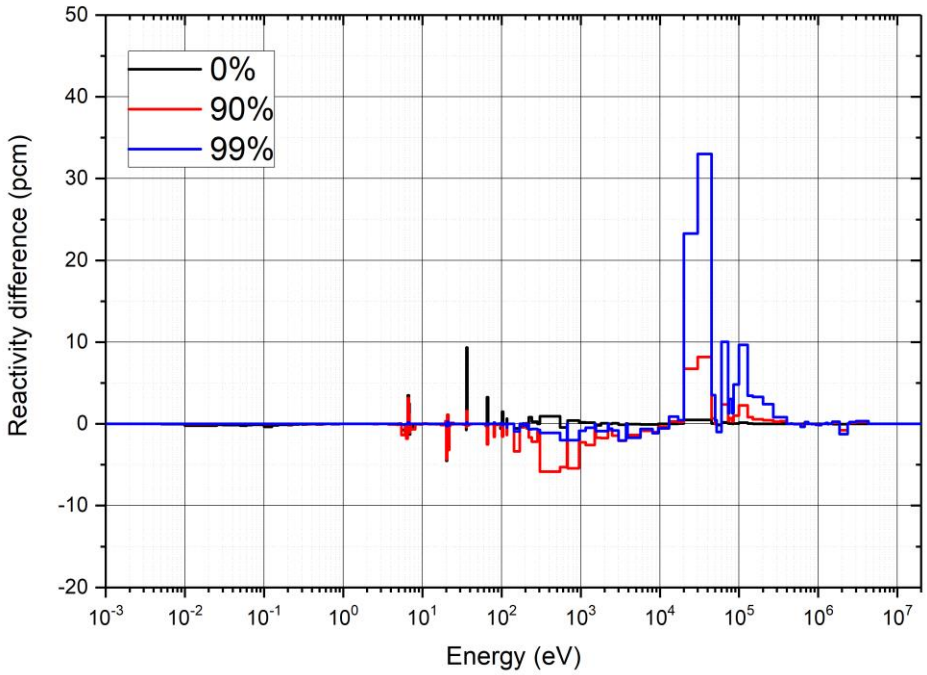

Figure 3.3.8. Reactivity differences due to the U^{238} capture cross section differences for UO_2 fuel pin problems with various void fractions.

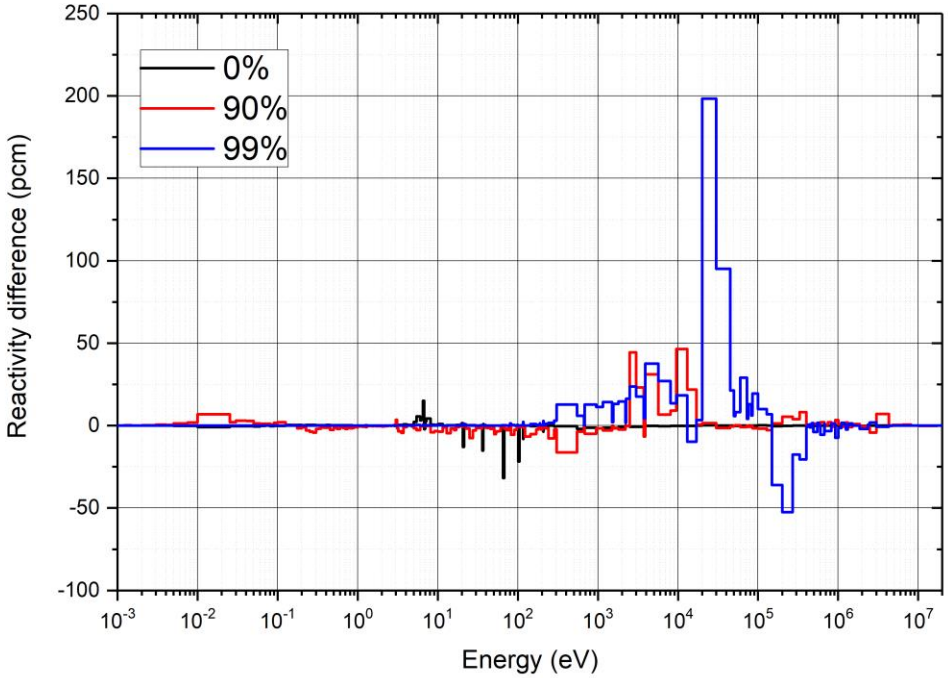

Figure 3.3.9. Reactivity differences due to the capture cross section and flux differences of U^{238} for UO_2 fuel pin problems with various void fractions.

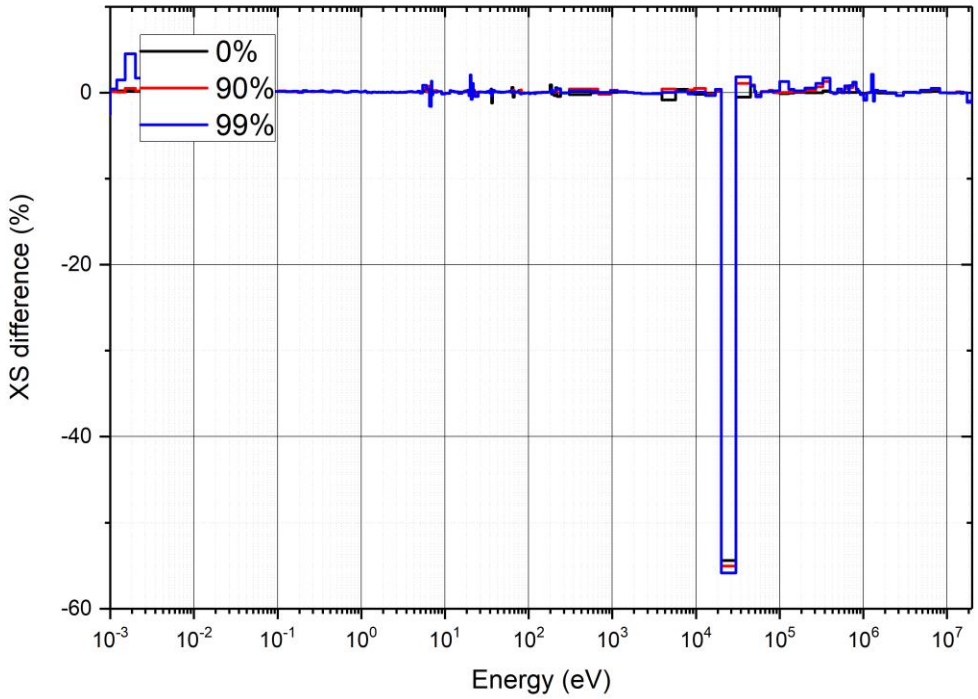

Figure 3.3.10.Comparison of U^{238} fission cross section differences in MG-KENO and MCNP for UO_2 fuel pin problems with various void fractions.

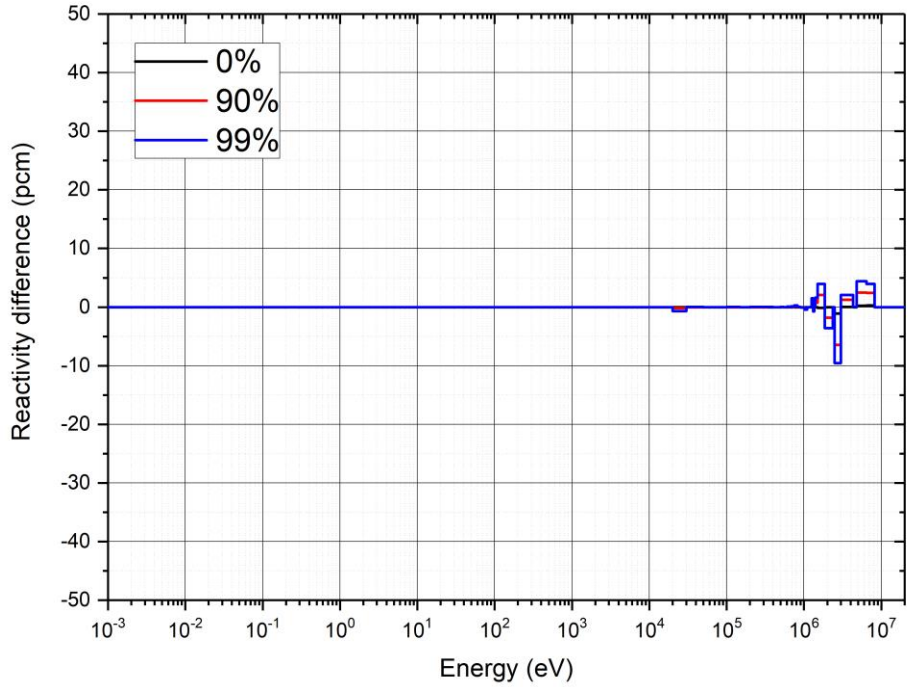

Figure 3.3.11. Reactivity differences due to the fission cross section differences of U^{238} for UO^2 fuel pin problems with various void fractions.

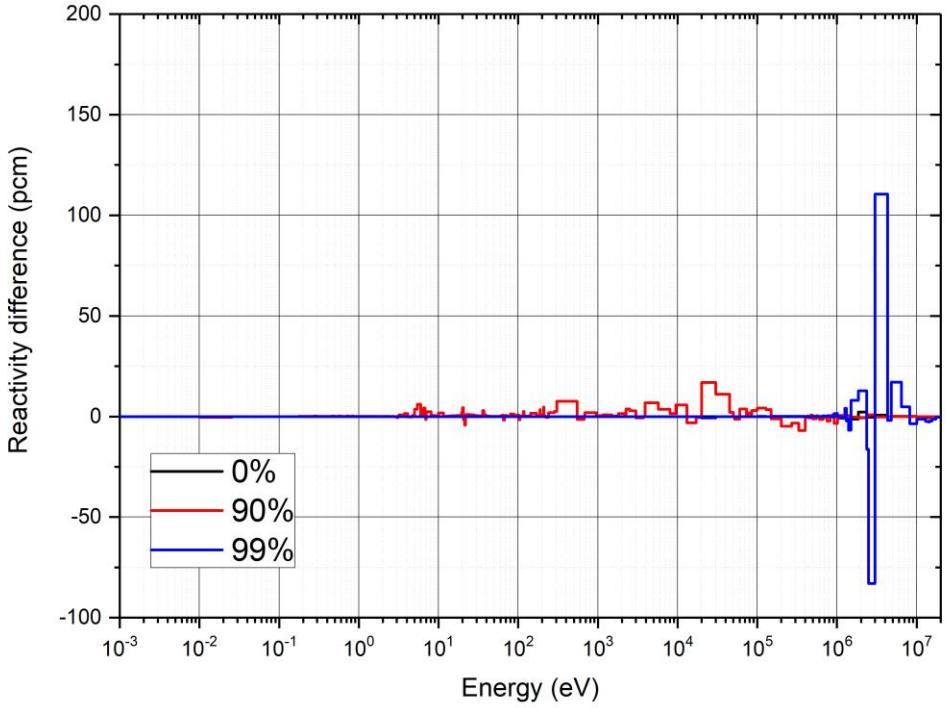

Figure 3.3.12. Reactivity differences due to the fission cross section and flux differences of U^{238} for UO_2 fuel pin problems with various void fractions.

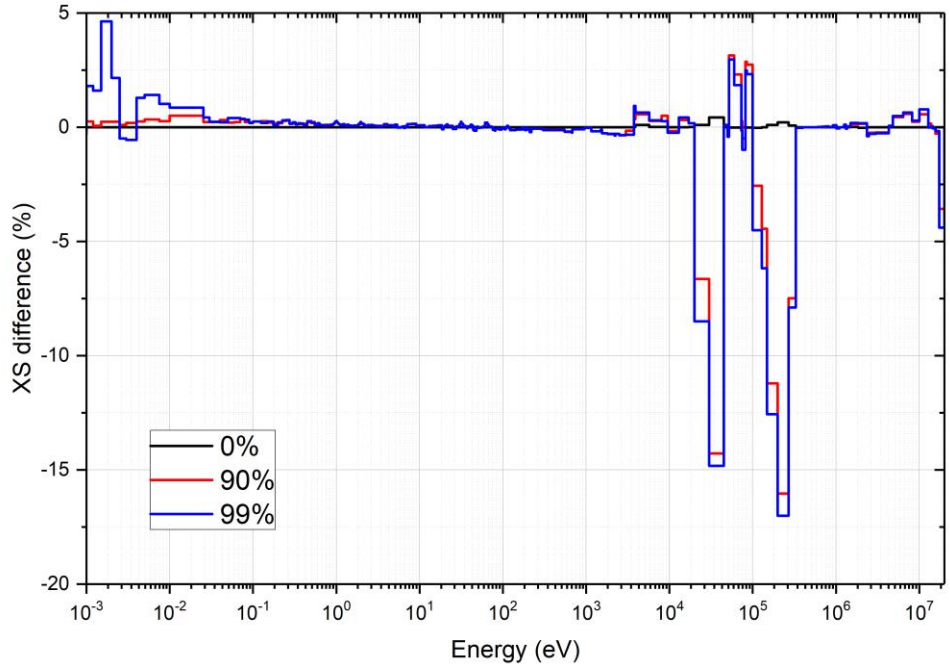

Figure 3.3.13. Comparison of Zr^{90} capture cross section differences in MG-KENO and MCNP for UO_2 fuel pin problems with various void fractions.

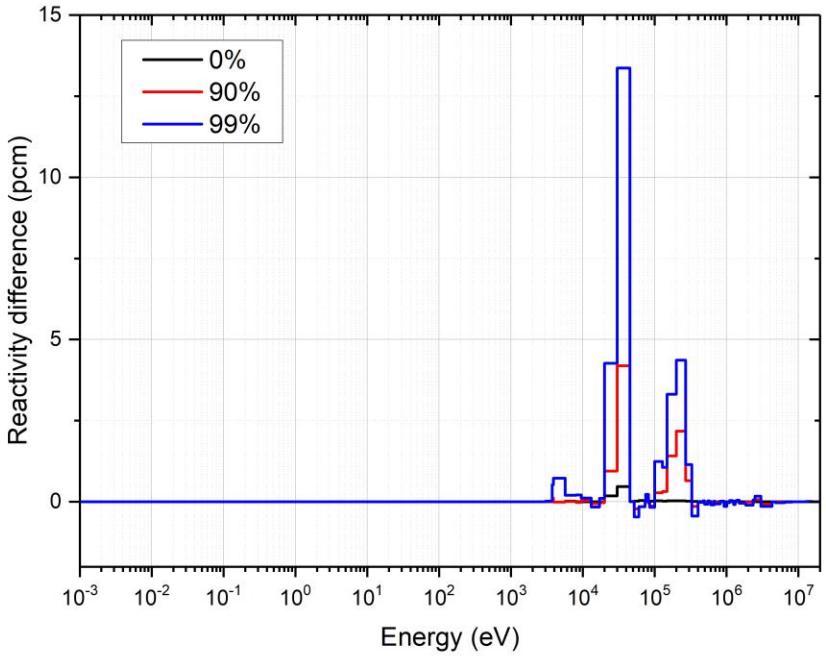

Figure 3.3.14. Reactivity differences due to the capture cross section differences of Zr^{90} for UO_2 fuel pin problems with various void fractions.

Figure 3.3.15 shows the capture and fission cross section errors of U^{238} and Pu^{239} for the ABTR problem. Figure 3.3.16 shows the direct effects of these cross section errors on the reactivity error, and Figure 3.3.17 shows the reactivity error caused by the reaction rate errors of these reactions. Figure 3.3.18 compares the cross section errors of Na^{23}, Fe^{56}, and Zr^{90} capture cross sections of ABTR. Similarly, Figure 3.3.19 shows the U^{238}, Pu^{239}, and Pu^{241} cross section errors of the MSR problem, and Figure 3.3.20 shows the direct effects of these cross section errors on the reactivity error, and Figure 3.3.21 shows the reactivity error caused by the reaction rate errors of these reactions. Figure 3.3.22 shows the Cl^{35} absorption cross section errors of the MSR problem, and Figure 3.3.23 shows the reactivity error caused by the reaction rate errors of Cl^{35} capture.

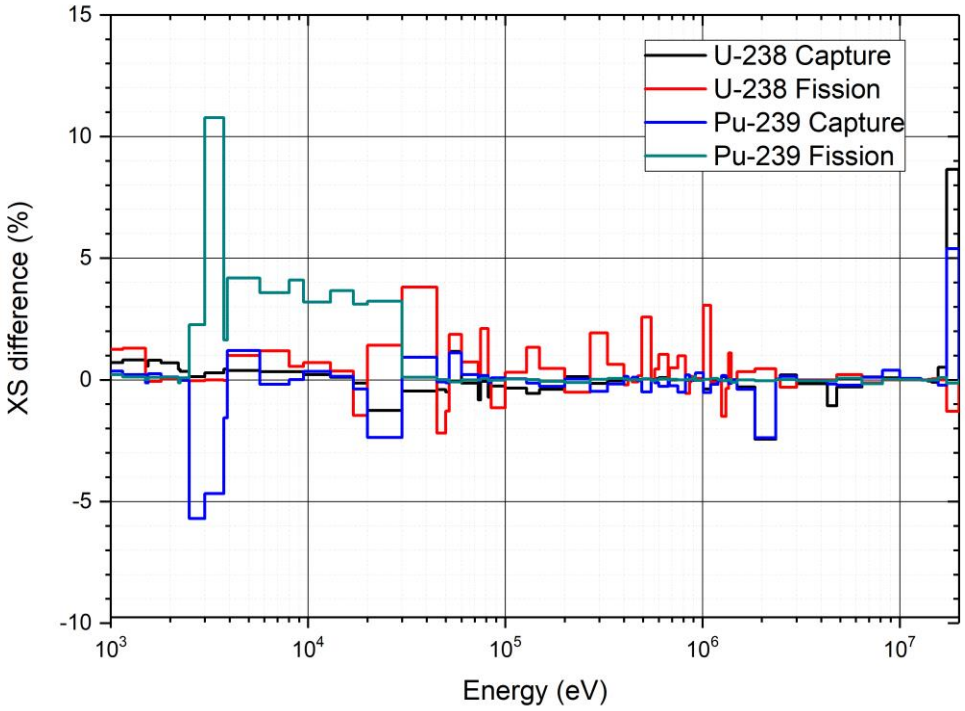

Figure 3.3.15. Comparison of U^{238} and Pu^{239} cross section differences in MG-KENO and MCNP for the ABTR problem.

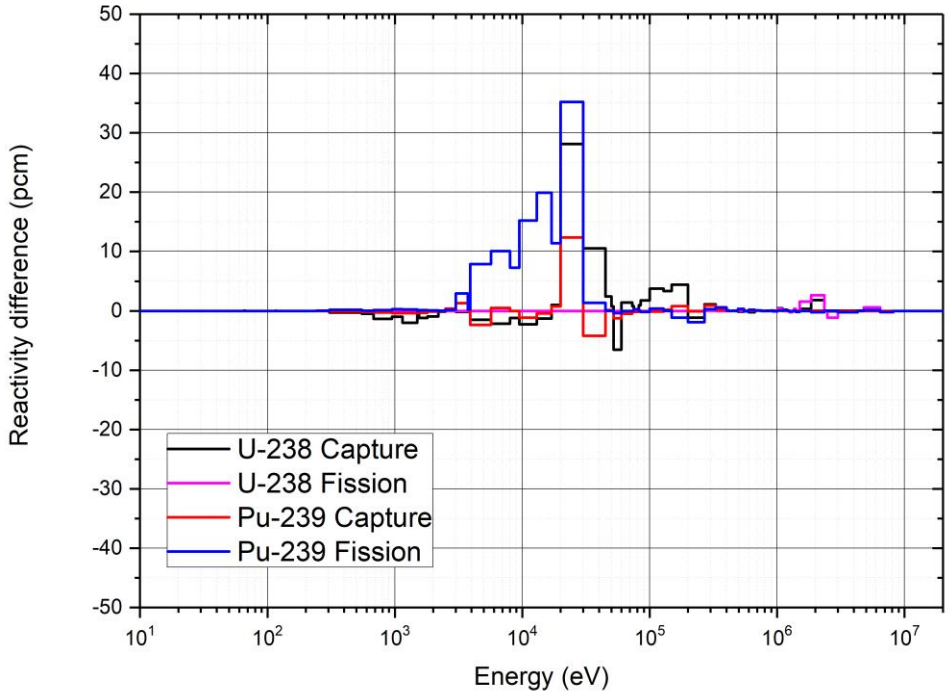

Figure 3.3.16. Reactivity differences due to the cross section differences of U^{238} and Pu^{239} for the ABTR problem.

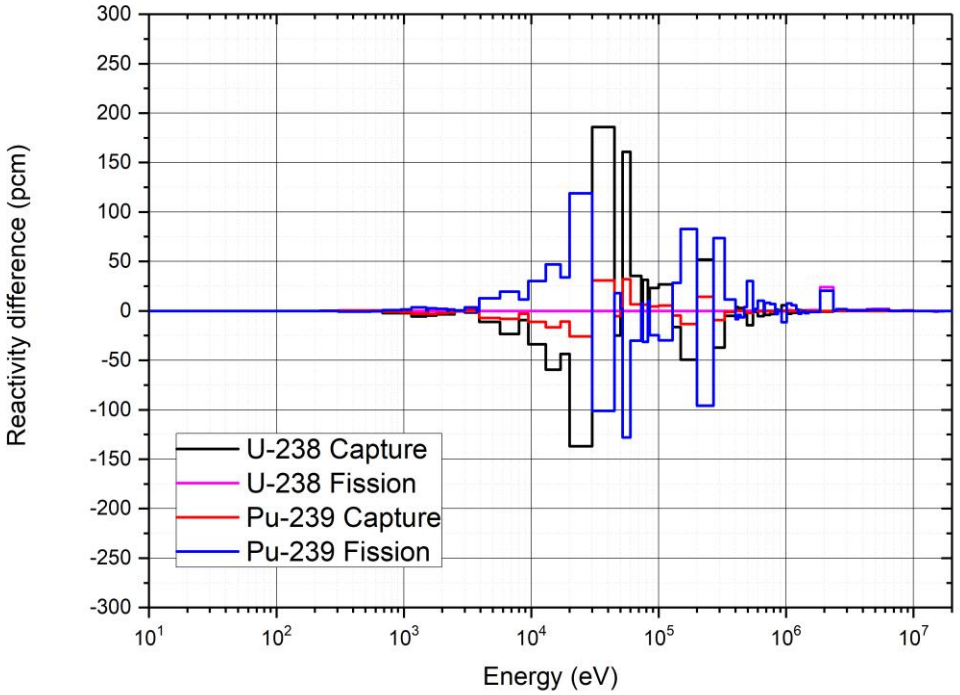

Figure 3.3.17. Reactivity differences due to the cross section and flux differences of U^{238} and Pu^{239} for the ABTR problem.

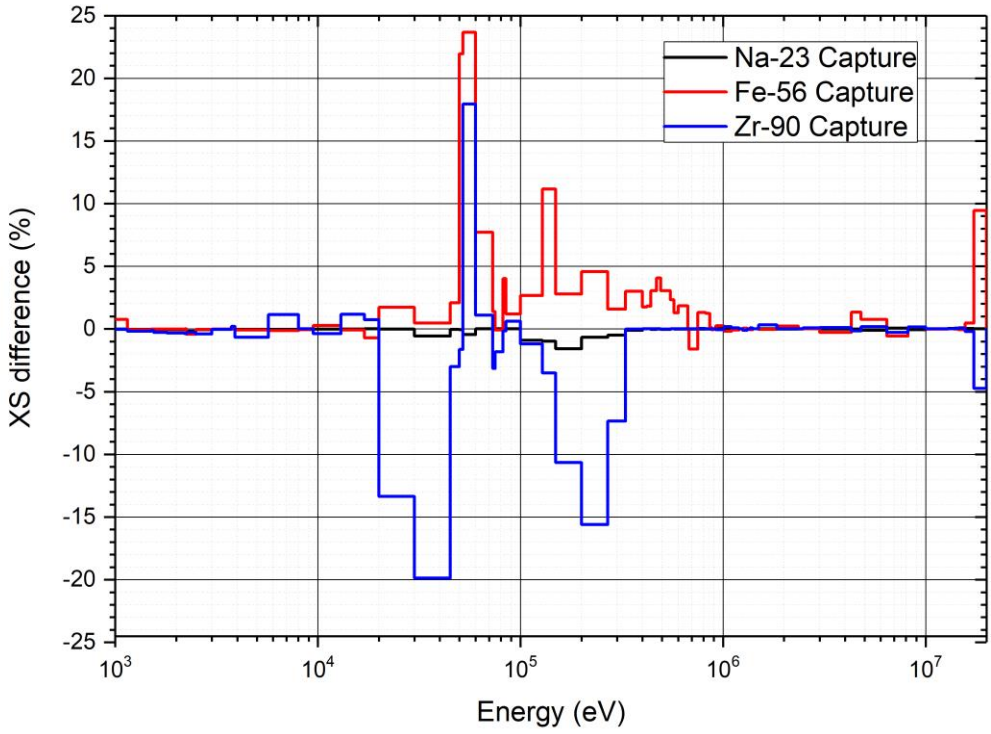

Figure 3.3.18. Comparison of Na^{23}, Fe^{56}, and Zr^{90} cross section differences in MG-KENO and MCNP for the ABTR problem.

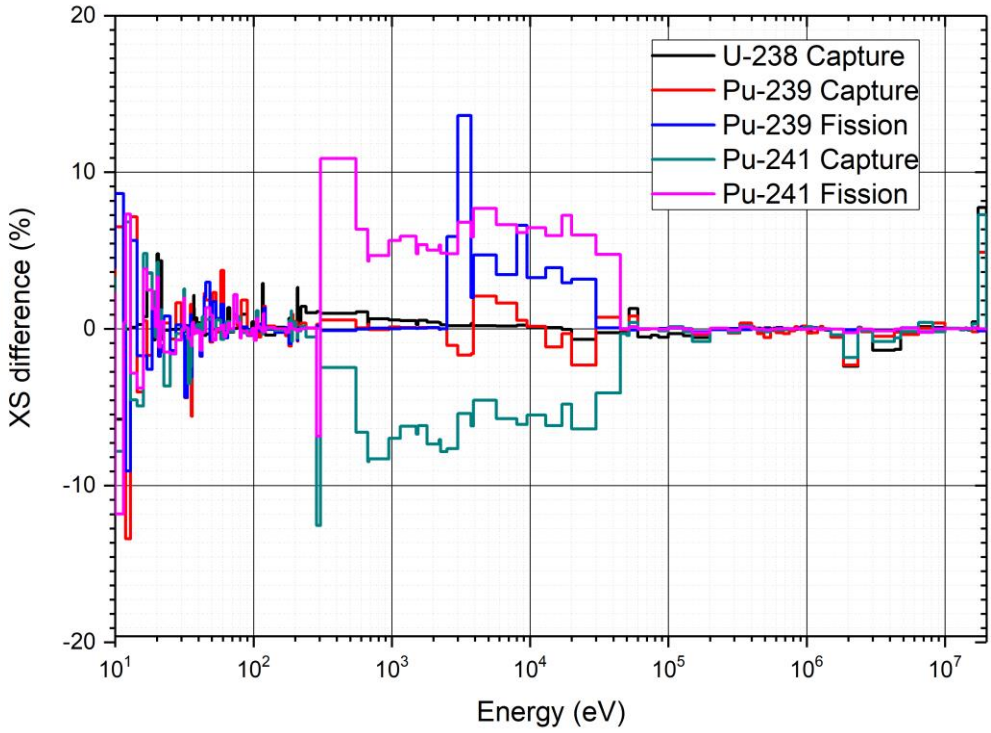

Figure 3.3.19. Comparison of U^{238}, Pu^{239}, and Pu^{241} cross section differences in MG-KENO and MCNP for the MSR problem.

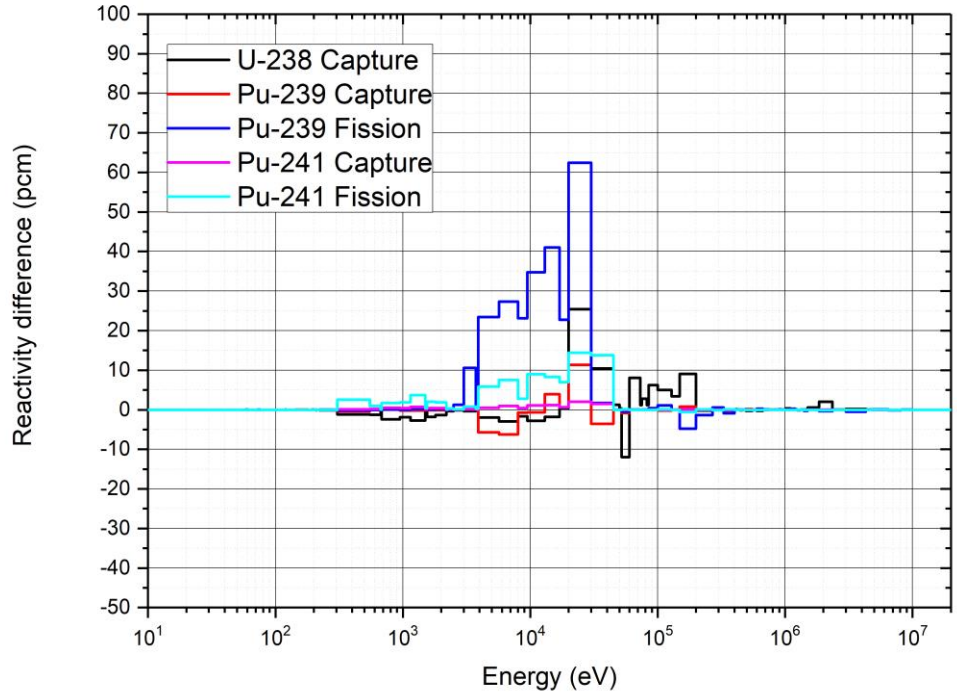

Figure 3.3.20. Reactivity differences due to the cross section differences of U^{238}, Pu^{239}, and Pu^{241} for the MSR problem.

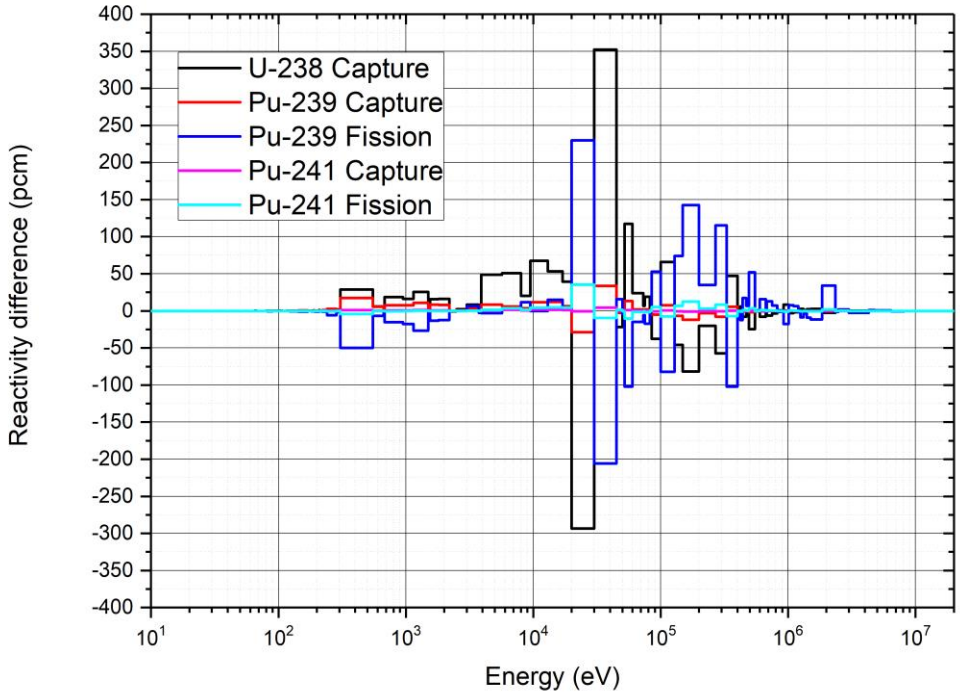

Figure 3.3.21. Reactivity differences due to the cross section and flux differences of U^{238}, Pu^{239}, and Pu^{241} for the MSR problem.

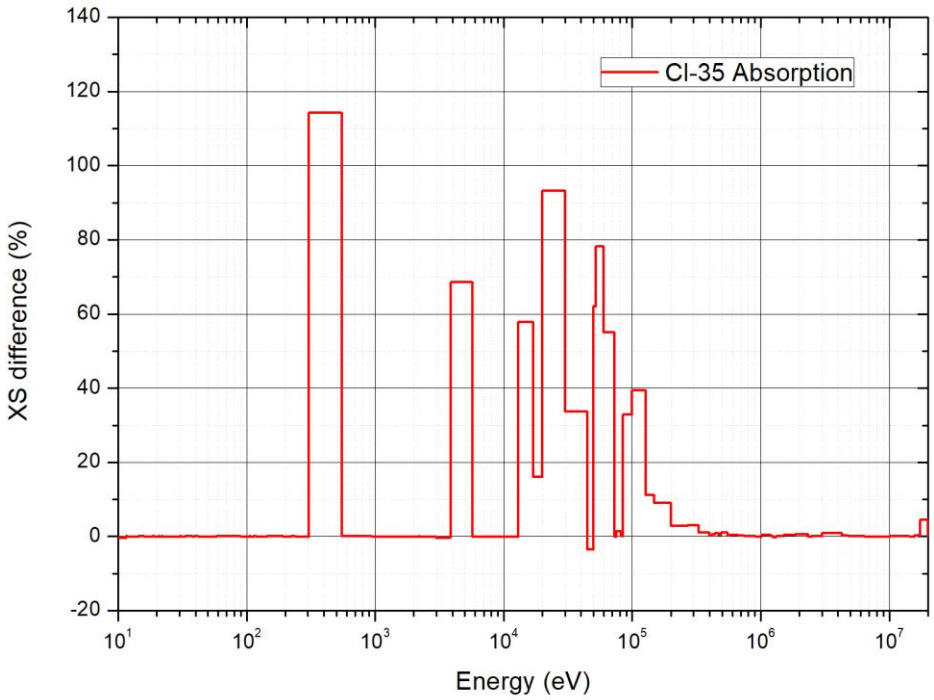

Figure 3.3.22. Absorption cross section differences of Cl^{35} between MG-KENO and MCNP for the MSR problem.

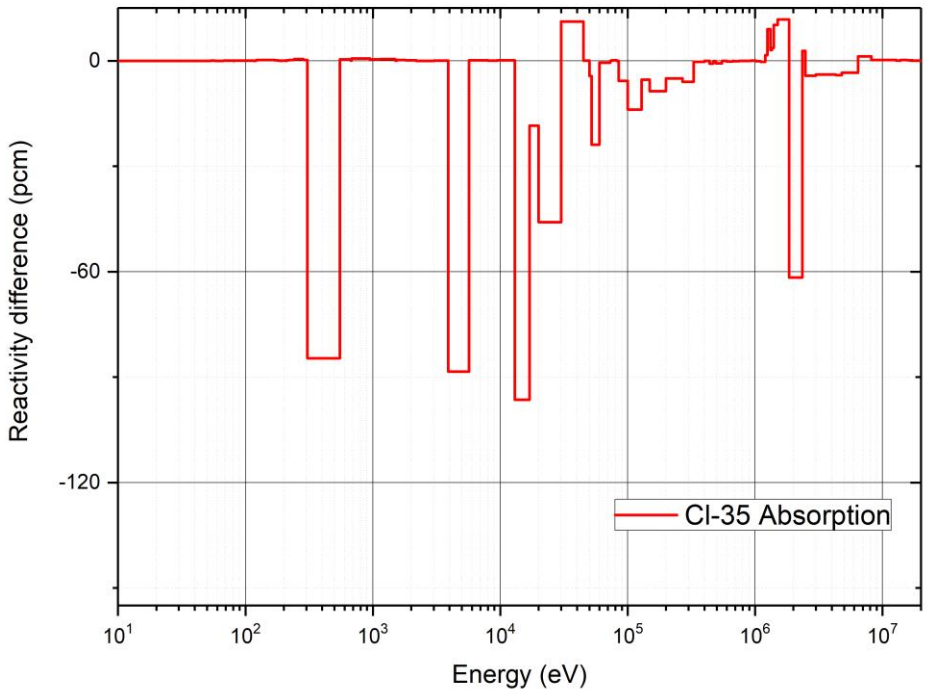

Figure 3.3.23. Reactivity differences due to the absorption cross section and flux differences of Cl^{35} for the MSR problem.

The cross section error plots show three distinct energy ranges of noticeable errors:the thermal energy range (–0.01–5 eV) for heavy isotopes, the URR energy range in CENTRM (–2.25–20 keV), and the fast energy range (> 20 keV). Following the standard SCALE procedure, the effective self-shielded cross sections for the URR and fast energy groups are determined by the Bondarenko approach using the resonance cross section tables provided in the AMPX MG library. URR energy ranges for major isotopes are provided in Table 3.3.3.

Table 3.3.3 URR energy range for major isotopes

Isotope	URR energy (keV)	Isotope	URR energy (keV)
U^{235}	2.25–25	Pu^{240}	5.7–40
U^{238}	20–149	Pu^{241}	0.3–40.2
Pu^{239}	2.5–30	Pu^{242}	0.9–44.7
Zr^{90}	53.5–100	—	

Although the U^{235} capture and fission reactions at thermal groups are the primary error sources for the PWR problem, the U^{238} capture reaction and the U^{235} capture and fission reactions at fast groups are the dominant error sources for the highly voided BWR cases, where hard neutron spectra due to higher void fractions amplify the reaction rate errors in the fast energy range. Comparisons between the reactivity error plots with and without including flux errors provide the contribution of scattering matrix errors to the reactivity error. These comparisons suggest that part of the reaction rate errors in fast groups are caused by the scattering matrix errors produced by the SCALE procedure.

Notably, the BWR problems with highly voided fractions (≥90%) and fast reactor problems show noticeable discrepancies in cross sections and reaction rates in the URR energy groups for U^{235}, U^{238}, Pu^{239}, and Pu^{241}. Also, for fast-spectrum cases, the energy ranges of noticeable cross sections errors of heavy nuclides clearly overlap the energy ranges of high cross section errors of intermediate-weight nuclides. For the highly voided BWR and fast reactor problems, heavy nuclide cross section errors are also noticeable in URR and very high energy groups, which have insignificant cross section errors for intermediate-weight nuclides. Reactivity error cancellation between U^{235} capture and fission reactions in thermal energy groups reported in [Kim17] is also observed. The noticeable errors of thermal capture and fission cross sections of U^{235} observed in coarse group structure are considered to be due to poor thermal scattering matrices. Figure 3.3.21 shows significant errors in the Cl^{35} absorption cross sections, causing large a large contribution to reactivity error.

4 IDENTIFIED PROBLEMS AND CORRECTIONS

The benchmark calculations in Section 3 showed the limited applicability of the AMPX/SCALE package for fast-spectrum problem analyses. The reaction rate analysis also showed that there are significant error cancellations among different reactions at different energy ranges. In this section, the identified potential error sources will be investigated further and potential correction methods will be examined.

4.1 NORMALIZATION ISSUE IN PROBABILITY TABLES

In the URR region, the experimental resolution is larger than the width of the resonances, and individual resonance parameters cannot be extracted from cross section fitting. Therefore, the ENDF evaluation provides mean values for the resonance spacing, the probability distribution for the spacing (i.e., the Wigner distribution), the mean values for the resonance partial widths, and the distributions for the partial widths (chi-square distributions for various numbers of degrees of freedom) at the selected grid energies E*. The ENDF allows two different representations of URR data depending on the option called LSSF. When LSSF = 1, the resonance parameters are to be used to compute a self-shielding factor that is to be applied to the cross section in File 3. When LSSF = 0, the parameters are used to compute cross sections that are to be added to any possible background corrections that may be given in File 3. For example, in the ENDF/B-VII.1, LSSF = 1 for U^{235}, U^{238}, and Pu^{238}, whereas LSSF = 0 for $Pu^{239}$and Pu^{241}. The number of energy grid points, E*, provided in the ENDF data is often insufficient for accurate reconstruction of cross sections; therefore, the resonance parameters need to be computed at additional energy points according to the interpolation law defined in the format [Cse12].

The AMPX/SCALE code package uses the analytic probability table method for the MG cross section generation for URR groups. The probability table method has been used successfully used for treating UR self-shielding. This method is based on generating “ladders” of resonances using the statistical properties of the unresolved range. One ladder can be generated for a grid energy by randomly selecting a starting resonance energy and a set of widths for that resonance and then moving to the next higher resonance by randomly selecting the resonance energy and the corresponding widths. This process is continued until there is a long ladder of resonances. With a ladder of resonance parameters in place, cross sections are calculated using the single level Breit–Wigner formula at randomly selected energy points. Using the calculated cross sections, a probability distribution function for the total cross section is determined by accumulating the hits in a predefined total cross section bins. However, using an insufficient number of ladders could result in average cross sections that differ from the expected infinitely dilute averages computed directly from the resonance parameters. Therefore, the average table cross sections in probability tables are normalized so that the calculated infinite dilute cross section is equal to the infinite dilute cross section in File 3.

Recently, AMPX probability tables were reported to have a normalization issue, resulting in a reactivity bias. New probability tables were generated with the ENDF/B-VII.1 data, and the ENDF/B-VII.0 data were used for a few isotopes. To investigate the effects of the probability table errors, the ENDF/B-VII.1 252-group AMPX MG libraries were regenerated using the new probability tables. The eight benchmark problems in

Table 3.0.1 were reanalyzed with the new 252-group library, and the results were compared with the results obtained with the current 252-group library.

Table 4.1.1 compares the MG-KENO eigenvalues obtained with the old and new probability tables with the MCNP6 reference values. As shown in Table 4.1.1, the replaced probability tables reduced the eigenvalue error of the MSR problem from 536 pcm to 389 pcm, but otherwise the tables did not show any noticeable improvement for other problems.

Table 4.1.1 Eigenvalues of MCNP6 and MG-KENO obtained with old and new probability tables for various pin cell problems

Fuel	Case	k-infinity				
		MCNP	MG-KENO (252-group)			
			Old PT	Diff. (pcm)	New PT	Diff. (pcm)
PWR	A1	1.43582 (6)	1.43436 (9)	−146 (10)	1.43432 (16)	−150 (70)
BWR	B1	1.39488 (6)	1.39337 (13)	−151 (14)	1.39332 (18)	−156 (19)
	B3	1.32518 (6)	1.32395 (16)	−123 (18)	1.32396 (16)	−122 (17)
	B3	1.24258 (6)	1.24159 (18)	−99 (19)	1.24137 (15)	−121 (16)
	B4	1.00980 (6)	1.01145 (12)	165 (13)	1.01165 (11)	185 (13)
	B5	0.91266 (4)	0.91920 (10)	654 (11)	0.91900 (8)	634 (10)
ABTR	C1	1.60150 (4)	1.60491 (12)	341 (13)	1.60467 (14)	317 (15)
MSR	D1	1.13927 (1)	1.14463 (7)	536 (7)	1.14316 (6)	389 (7)

Table 4.1.2 compares the effects on reactivity error of the reaction rate errors determined with the old and new probability tables for the MSR problem. This table shows that the new probability tables of Pu^{241} are the main contributor to the improved MSR eigenvalue. Figure 4.1.1 compares the relative deviations of the U^{238} capture cross sections and Pu^{241} fission cross sections of MG-KENO before and after the correction of the normalization issue of probability tables from the tallied MCNP cross sections. This figure shows that the new probability tables significantly reduce the discrepancies of Pu^{241} fission cross sections in the URR range but only slightly for the U^{238} capture cross sections.

It is also noted from Table 4.1.2 that the fast-spectrum problems B4, C1, and D1 still show a large eigenvalue discrepancy from the MCNP reference solution. These large eigenvalue discrepancies could be caused by the errors in principal cross sections and scattering matrices in the fast energy region above the URR region. These cross section errors can be attributed to the limitation of Bondarenko approach in a coarse group structure of AMPX/SCALE code package.

Table 4.1.2 Comparison of the effect of probability tables for MSR problem

PT	$\Delta\rho$ [pcm]		Nuclide	XS/Flux effect [pcm]		
	Code	RR		RR_{cap}	RR_{fis}	SUM
Old PT	411 (5)	409	92235	4	−6	409
			92238	485	43	
			94239	125	86	
			94240	11	5	
			94241	18	53	
			94242	4	4	
			11023	4	0	
			17035	−426	0	
New PT	299 (5)	299	92235	4	−6	299
			92238	455	44	
			94239	125	88	
			94240	14	3	
			94241	5	−20	
			94242	8	3	
			11023	4	—	
			17035	−427	—	

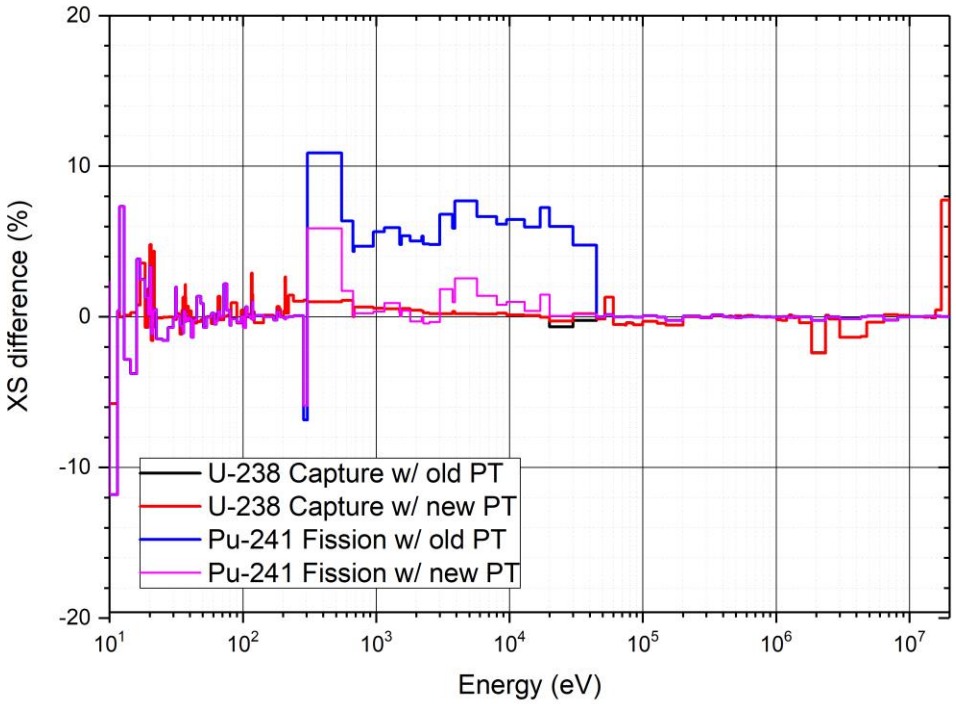

Figure 4.1.1. Cross section differences of U^{238} and Pu^{241} using old and new probability tables for MSR problem.

4.2 LIMITATION OF BONDARENKO APPROACH IN A COARSE GROUP STRUCTURE

In the standard SCALE procedure, the BONAMI module first calculates self-shielded cross sections for all nuclides and energy groups using the NR or IR approximation and the Bondarenko approach. Then the cross sections below the URR region are replaced by the self-shielded cross sections computed by CENTRM PW transport calculations. The Bondarenko approach based on the IR approximation assumes that the self-shielded MG flux spectrum at target temperature can be determined by solving the following slowing-down equation [Sca16]:

$$\left[\sigma_t^r(E,T)+\sigma_0^r(E,T)\right]\phi^r(E,T)=\frac{1}{N^r}S^r(E,T)+\frac{1}{N^r}\sum_{j\neq r}\lambda_g^j\sum_p^j C(E) \tag{4.2.1}$$

where N^r and σ_t^r are the number density and total cross section of a resonance nuclide r, respectively, and S^r is the elastic scattering source due to scattering with the resonance nuclide r. $\sum_p^j$ and λ_g^j are the potential scattering cross section and IR parameter in group g of nuclide j, respectively, and $C(E)$ is a smooth function of the asymptotic flux in a homogeneous medium. σ_0^r is the background cross section of nuclide r in the homogeneous medium defined as

$$\sigma_0^r(E,T)=\frac{1}{N^r}\sum_{j\neq r}\left(\sum_a^j(E,T)+\lambda_g^j\sum_s^j(E,T)\right) \tag{4.2.2}$$

The cross sections in Eqs. (4.2.1) and (4.2.2) are assumed to be group-averaged constants in a group. By solving Eq. (4.2.1) for a selected set of background cross section values, self-shielded group cross sections are determined. Self-shielding factors are determined by dividing the self-shielding cross sections by the infinite dilute cross section and tabulated in a AMPX MG library along with the infinite dilute cross section. For a given target system, BONAMI computes the background cross section σ_0^r using Eq. (4.2.2) and interpolates the Bondarenko data in the AMPX library to obtain the self-shielding factor corresponding to the calculated σ_0^r value. The AMPX MG master library includes the self-shielding factor and infinite dilute cross section for the following five reaction types: total, radiative capture, fission, within-group scattering, and elastic scattering. Since the background cross section is determined using the self-shielded cross section of other nuclides, the Bondarenko iteration are performed to account for resonance interference effects.

It has been proven that the Bondarenko approach in the current 252-group structure works reasonably well for representing the heavy resonant nuclides in thermal LWR systems. However, its application to a fast-spectrum reactor where all the nuclides are resonant is limited because of the limitation of Bondarenko iteration and the approximations used in deriving Eq. (4.2.1). Since the Bondarenko method treats only one nuclide at a time, significant cross section errors can be induced in certain groups

where multiple nuclides have large resonances, as can be seen below 10 keV in Figure 3.3.15 of Section 3.3, which shows the relative discrepancies of MG-KENO cross sections from the tallied MCNP cross sections. Furthermore, the asymptotic 1/E spectrum used in deriving Eq. (4.2.1) is not adequate for fast-spectrum problems. The NR or IR approximation is not applicable to the broad scattering resonances of intermediate-weight nuclides, either. In addition, the broad scattering resonances cannot be well represented by constant background cross sections in the 252-group structure.

For example, in Figure 4.2.1 that shows U^{238}, O^{16} and Zr^{90} total cross sections of the BWR problem B5, it can be seen that the broad scattering resonances of Zr^{90} are overlapped with the resolved and UR of U^{238} and they cannot be treated as constant background cross sections for U^{238} cross section self-shielding. By comparing Figures 3.3.1–3.3.14 that show the cross section and reactivity errors for the LWR benchmark problems, it can be clearly seen that the observed reactivity discrepancies are mainly caused by the broad scattering resonances of zirconium and their interactions with heavy nuclide resonances. It is noted that the reaction rate errors in the vicinity of broad resonances of oxygen is much smaller than those of zirconium since the AMPX used a calculated C(E) with CENTRM for hydrogen and oxygen while the NR approximation is used to represent the flux spectrum for masses below A = 40 [Sca16].

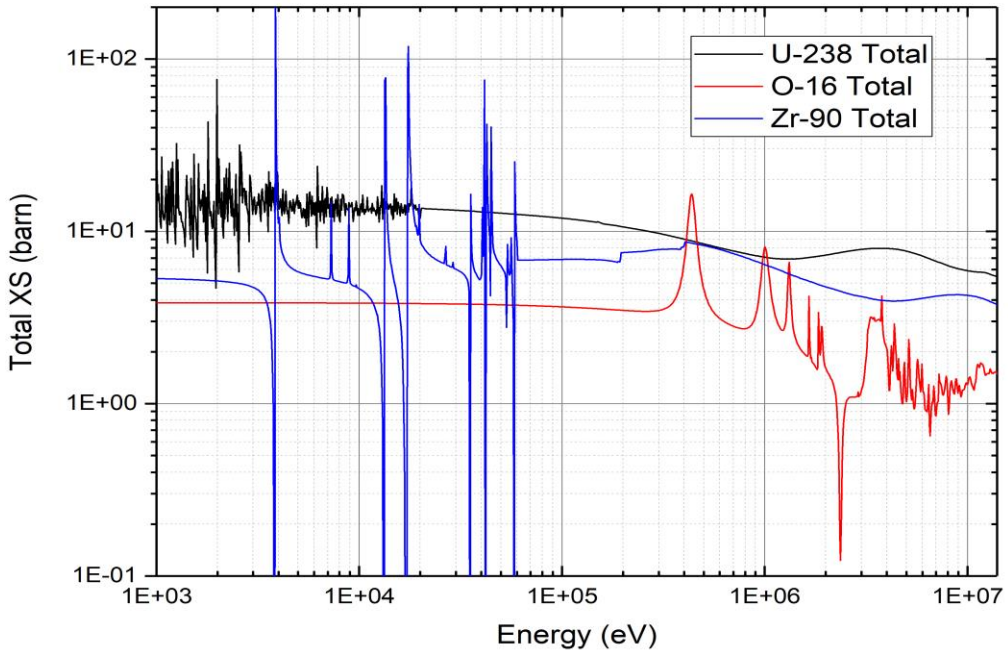

Figure 4.2.1. MCNP 1,585-group total cross section of U^{238}, O^{16}, and Zr^{90} for 99% void BWR.

A similar trend was found for the ABTR benchmark problem. Figure 4.2.2 shows the total cross section of Pu^{239}, Na^{23}, and Fe^{56} of the ABTR problem. Comparison of Figure 4.4.2 with Figure 3.3.17 suggests that the observed reactivity discrepancy is mainly caused by the broad resonances of Fe^{56}, although Fe^{56} cross section errors do not contribute much

to the reactivity discrepancy. Therefore, it can be concluded that the constant background cross sections in 252-group level and the asymptotic flux spectrum are not adequate for fast-spectrum analysis.

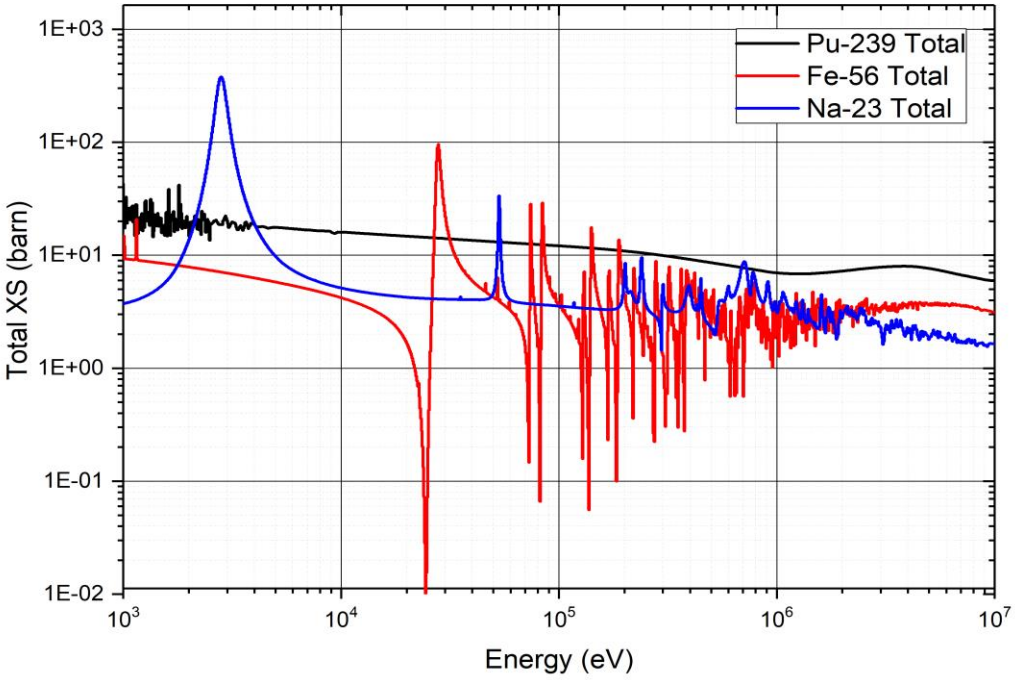

Figure 4.2.2. MCNP 1,585-group total cross section of Pu^{239}, Fe^{56}, and Na^{23} for the ABTR problem.

To investigate the accuracy of scattering matrices, P0 scattering matrices of the AMPX 252-group library were compared to the reference scattering matrices generated with the MC code McCARD developed at Seoul National University [Shi12]. The McCARD calculation was performed with 5,000 active cycles and 1,000,000 histories per cycle so that the relative uncertainties are less than 0.5% for most of the scattering matrix elements. Figure 4.2.3 compares the P0 scattering matrix of U^{238} in the 252-group AMPX MG library with the tallied scattering matrix from the McCARD calculation for the highly voided BWR problem B5. Large relative errors are observed in the fast energy groups from group 20 (1.3 MeV) to 60 (5.7 keV), which lead to notable discrepancies in the flux spectrum.

These observations suggest the refinement of the energy groups (1) to represent broad scattering resonances of intermediate-weight nuclides accurately by a piecewise constant function, (2) to improve the accuracy of Bondarenko iteration among multiple resonant nuclides, and (3) to improve the accuracy of scattering matrices. To examine the performance of refined energy groups, a UFG AMPX library was genearted in the 1,585-group structure discussed in Section 2.2 using the AMPX/SCALE code packages and procedures. With this new 1,585-group library, the eight benchmark problems were reanalyzed. To separate the effect of the refined group structure, the new probability tables were used for both the 252- and 1,585-group libraries. Table 4.2.1 compares the MG-KENO eigenvalues obtained with the 252- and 1,585-group libraries with the

reference MCNP results. The use of the UFG library remarkablely improves the eigenvalue accuracy for the fast-spectrum problems B4, B5, C1, and D2. As mentioned in Section 3.3, the remaining errors for A1, B1, B2, and B3 cases might be due to poor thermal scattering matrices in the coarse group structure [Kim17], and the remaining MSR problem errors are due to the cross section discrepancies of Cl^{35} isotope at high energy range.

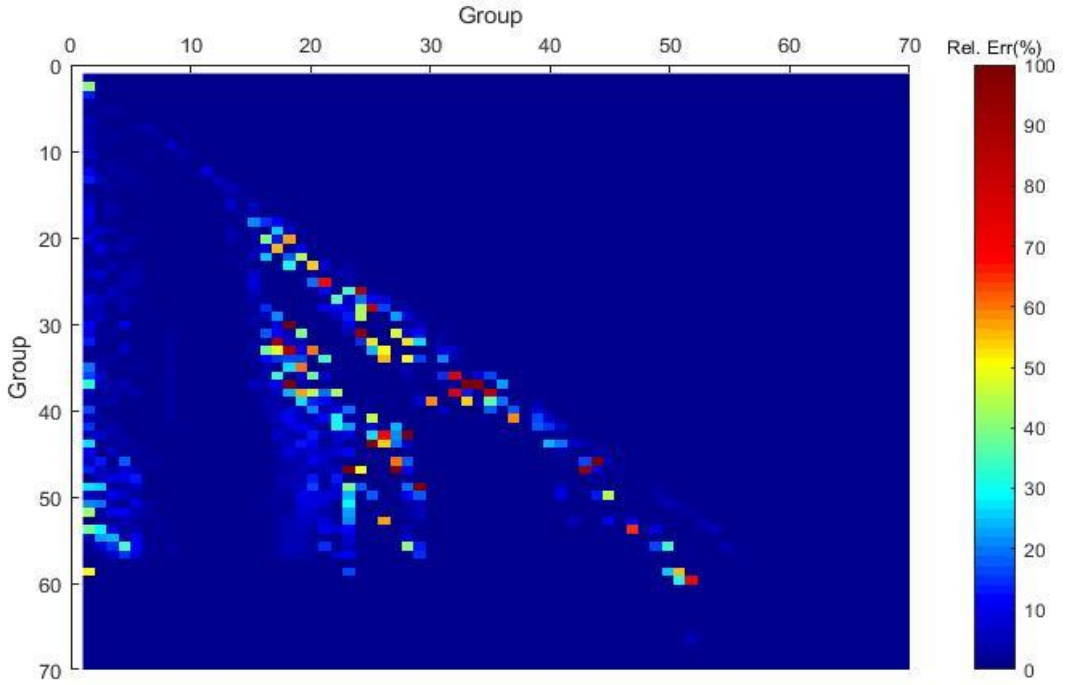

Figure 4.2.3. Comparison of P0 scattering matrix of U^{238} between the 252-group AMPX MG library and McCARD for 99% void BWR.

Table 4.2.1 Comparison of eigenvalue between 252- and 1,585-group AMPX MG libraries for various pin cell problems

Fuel	Case	k-infinity				
		MCNP	MG-KENO			
			252-group	Diff (pcm)	1,585-group	Diff (pcm)
PWR	A1	1.43582 (6)	1.43432 (16)	−150 (70)	1.43413 (17)	−169 (18)
BWR	B1	1.39488 (6)	1.39332 (18)	−156 (19)	1.39336 (16)	−152 (17)
	B3	1.32518 (6)	1.32396 (16)	−122 (17)	1.32365 (17)	−153 (18)
	B3	1.24258 (6)	1.24137 (15)	−121 (16)	1.24106 (18)	−152 (16)
	B4	1.00980 (6)	1.01165 (11)	185 (13)	1.00936 (11)	−44 (13)
	B5	0.91266 (4)	0.91900 (8)	634 (10)	0.91296 (10)	30 (12)
ABTR	C1	1.60150 (4)	1.60467 (14)	317 (15)	1.60075 (11)	−75 (12)
MSR	D1	1.13927 (1)	1.14316 (6)	389 (7)	1.13762 (7)	−165 (7)

4.3 SELF-SHIELDING OF RESONANCE-LIKE CROSS SECTIONS AT HIGH ENERGY GROUPS

As discussed in the previous section, AMPX MG master library provides the self-shielding factor and infinite dilute cross section for five major reactions. However, it was found that the resonance-like cross sections of some absorption reactions, such as (n,p) and (n,α), were not self-shielded properly by the AMPX/SCALE code package. The cross sections of these absorption reactions often vary smoothly over the entire energy range of interest in fission reactors, but they exhibit resonance-like variations for certain nuclides in keV to MeV ranges. As an example, Figure 4.3.1 shows the pointwise (n, p) cross section of Cl^{35}.

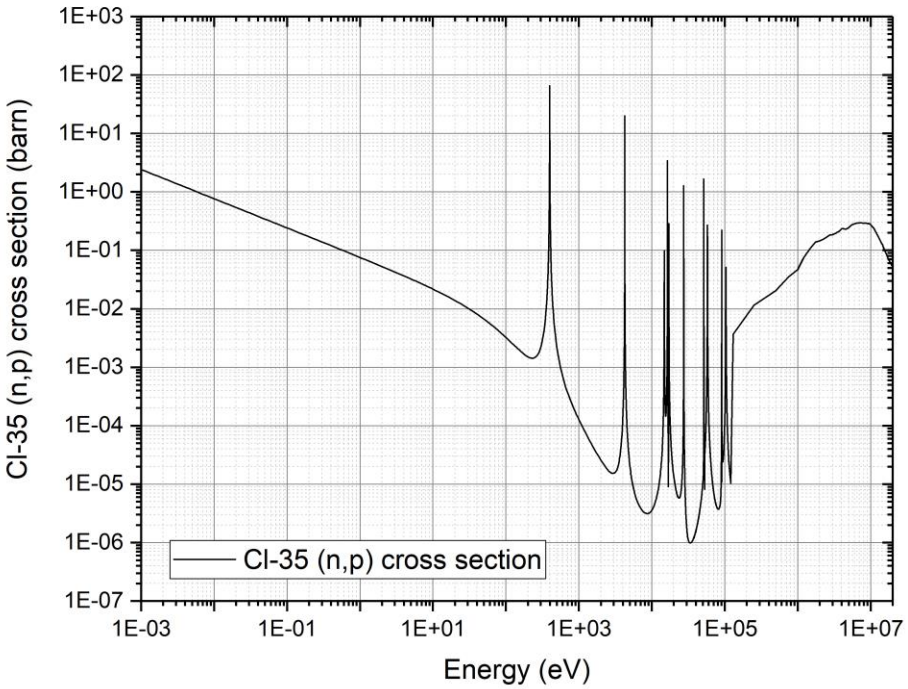

Figure 4.3.1. Point-wise (n,p) cross section of Cl^{35}.

The neglect of self-shielding effects in MG cross section generation introduces significant errors in MG cross sections as shown in Figure 3.3.22 for the absorption cross section of Cl^{35} [i.e., the sum of capture and (n,p)] in the MSR problem. These MG cross section errors introduce a significant error in reactivity as shown in Figure 3.3.23. Therefore, the AMPX/SCALE code package needs to be modified to implement a self-shielding capability for resonance-like cross sections at high energies.

5 ADOPTION OF ULTRA-FINE GROUP SLOWING-DOWN CALCULATIONS

In Section 3, it was observed that the AMPX 252-group library resulted in relatively large reactivity bias and groupwise reaction rate errors for the fast-spectrum problems. The reaction rate analysis showed that the main contributor to the reactivity bias is the cross section errors of heavy nuclides at high energy groups. These cross section errors are due to the limitation of Bondarenko approach in the 252-group structure, which is caused by the lack of 1/E asymptotic spectrum, strong interactions of multiple resonant nuclides, and broad resonances of intermediate-weight nuclides.

As discussed in Section 4.2, to examine the performance of refined energy groups, a UFG AMPX library was genearted in a 1,585-group structure using the AMPX/SCALE code packages and procedures discussed in Section 2.2. The new probability tables discussed in Section 4.1 were included, but the resonance-like cross sections of Cl^{35} (n,p) reaction were not self-shielded. Therefore, the reactivity error due to the Cl^{35} cross section errors would remain in the MSR problem.

5.1 PERFORMANCE OF NEW AMPX 1,585-GROUP LIBRARY

As shown in Table 4.2.1, the new 1,585-group AMPX library resulted in remarkable eigenvalue improvements for fast reactor problems B4, B5, C1, and D1. To investigate group-wise contributions, reaction rate analysis was also performed for the highly voided BWR problem B5, ABTR problem C1, and MSR problem D1. Comparing Table 5.1.1 with Table 3.3.1 and Table 5.1.2 with Table 3.3.2 shows the new AMPX 1,585-group library improved reaction rates significantly. For example, the reactivity error due to U^{238} capture reaction error was reduced from 543 to 53 pcm for the B5 case and from 485 to 51 pcm for the D1 case. The reactivity error in ABTR due to Pu^{239} fission reaction error is reduced from 142 to −12 pcm. These results indicate that the 1,585-group slowing-down calculation resulted in a significantly improved within-group flux distribution in each of the 252-groups compared to the approximate flux distribution obtained with the NR or IR approximation and subsequently produced significantly improved 252-group cross sections.

Figures 5.1.1–5.1.6 show the cross section errors and reactivity error caused by the reaction rate errors for the B5, C1, and D1 cases. By comparing Figure 5.1.1 with Figures 3.3.1, 3.3.4, 3.3.7, and 3.3.10, Figure 5.1.3 with Figure 3.3.15, and Figure 5.1.5 with Figure 3.3.19, it can be seen that the 252-group cross section errors above the RR region are significantly reduced by adopting the 1,585-group structure. The reactivity error results on Figures 5.1.2, 5.1.4, and 5.1.6 also show that the resulting 252-group reaction rates of MG-KENO agree well with the reference MCNP results except for the absorption reaction of Cl^{35}, which was caused by neglecting the self-shielding of (n,p) cross section. The maximum contribution to the reactivity error of a group reaction rate is reduced from 230 to 15 pcm for B5, and from 370 to 6 pcm for D1.

Table 5.1.1 Reaction rate analysis results of the new 1,585-group library for UO_2 fuel pin cell problem with various void fractions

Void	Case	$\Delta\rho$ (pcm)		Nuclide	XS/Flux effect (pcm)			XS effect (pcm)		
		Code	RR		RR_{cap}	RR_{fis}	SUM	RR_{cap}	RR_{fis}	SUM
0% (PWR)	A1	−82 (9)	−76	92235	15	−10	−76	−11	27	19
				92238	−79	−2		4	−1	
40%	B1	−78 (9)	−77	92235	15	−13	−76	−11	26	12
				92238	−77	−1		−2	−1	
70%	B2	−87 (10)	−84	92235	16	−19	−83	−12	27	5
				92238	−76	−5		−8	−2	
90%	B3	−99 (11)	−88	92235	16	−17	−87	−14	29	10
				92238	−79	−8		−23	−2	
90%	B4	−43 (12)	−39	92235	11	−26	−35	−13	22	−42
				92238	−9	−15		−48	−6	
				8016	—	—		−2	—	
				40090	5	—		5	—	
99%	B5	34 (12)	38	92235	−2	6	42	−2	−1	22
				92238	53	-27		22	−9	
				8016	−1	—		−2	—	
				40090	14	—		13	—	

Table 5.1.2 Reaction rate analysis results of the new 1,585-group library for ABTR and MSR problems

Void	Case	$\Delta\rho$ (pcm)		Nuclide	XS/Flux effect (pcm)			XS effect (pcm)		
		Code	RR		RR_{cap}	RR_{fis}	SUM	RR_{cap}	RR_{fis}	SUM
ABTR	C1	−29 (5)	−18	92235	—	—	−16	—	—	−10
				92238	4	−3		5	−1	
				94239	5	−13		3	−9	
				94240	—	—		—	—	
				40090	4	—		5	—	
				11023	−6	—		−6	—	
				26056	−7	—		−7	—	
				26054	—	—		—	—	
MSR	D1	−127 (5)	−121	92235	1	−3	−120	—	—	−207
				92238	51	—		−12	−3	
				94239	19	−33		−1	−9	
				94240	2	—		—	—	
				94241	—	2		−1	6	
				94242	−4	1		−6	—	
				11023	1	—		—	—	
				17035	−158	—		−182	—	

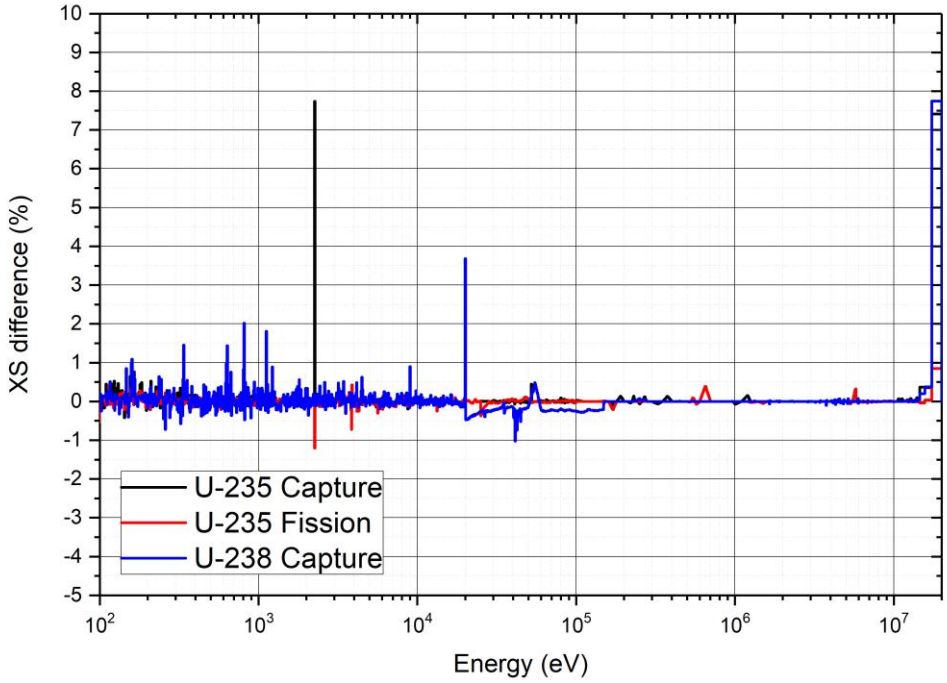

Figure 5.1.1. Cross section differences of U^{235} and U^{238} between MG-KENO and MCNP for 99% void BWR.

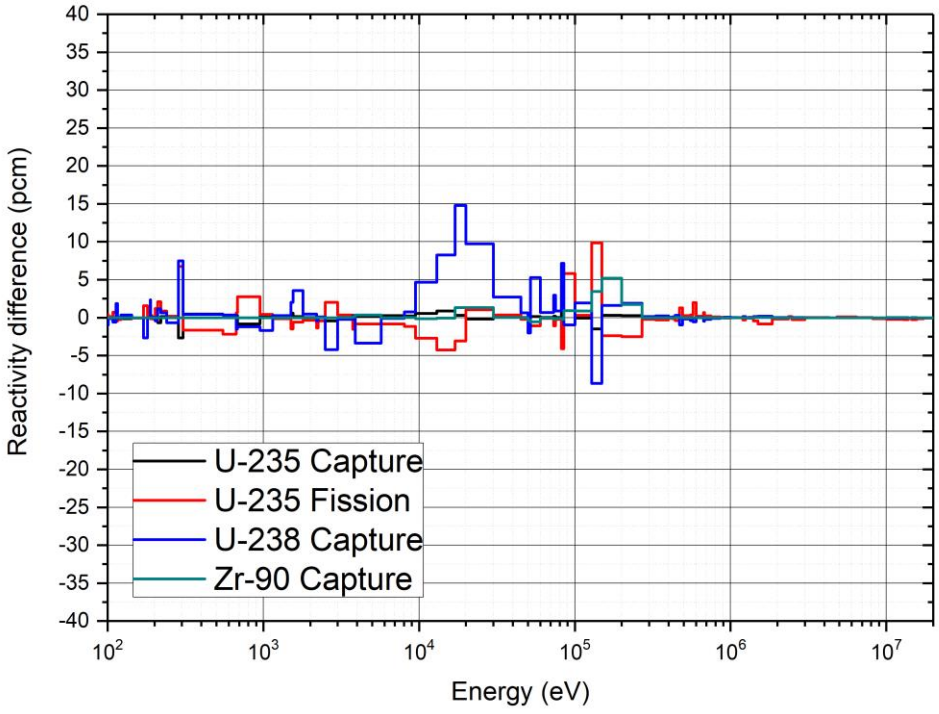

Figure 5.1.2. Reactivity differences due to the cross section and flux differences of U^{235}, U^{238}, and Zr^{90} for 99% void BWR.

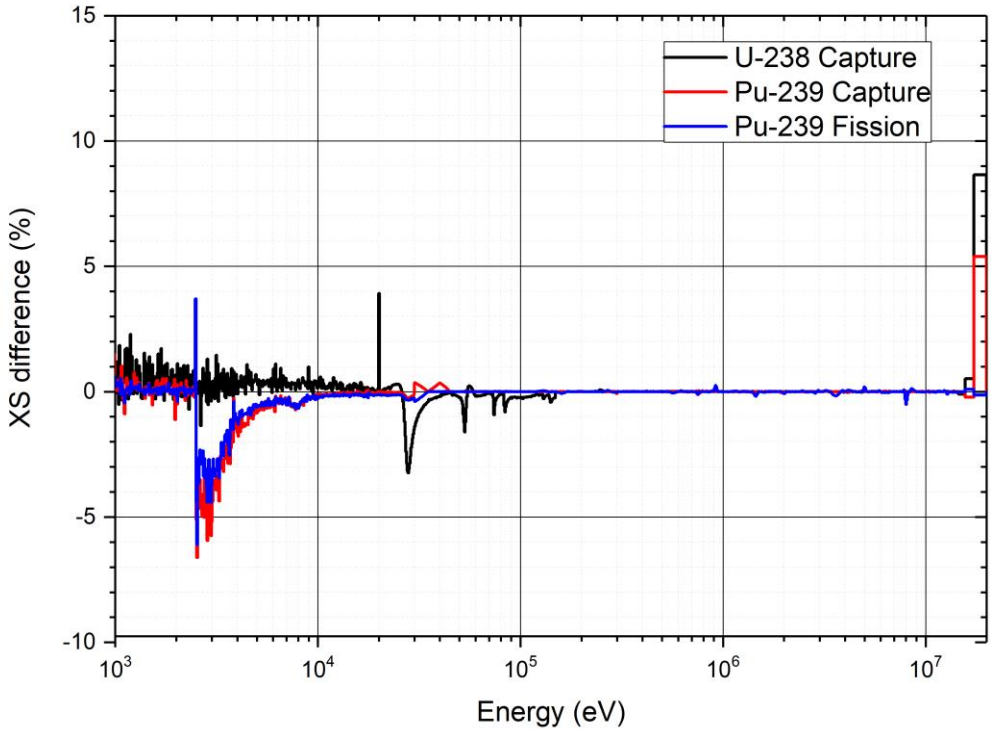

Figure 5.1.3. Cross section differences of U^{238} and Pu^{239} between MG-KENO and MCNP for the ABTR problem.

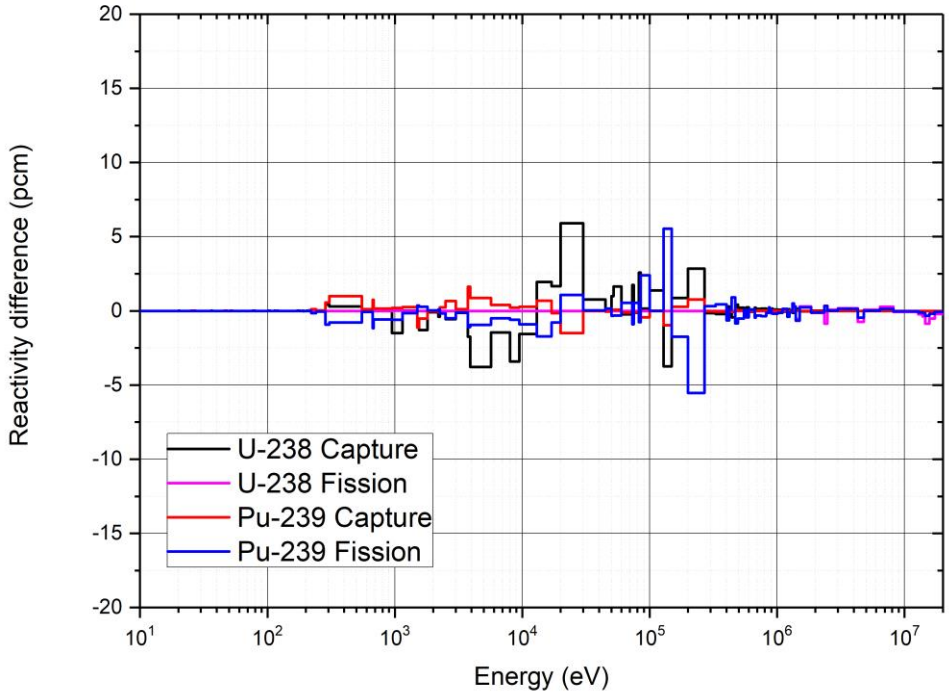

Figure 5.1.4. Reactivity differences due to the cross section and flux differences of U^{238} and Pu^{239} for the ABTR problem.

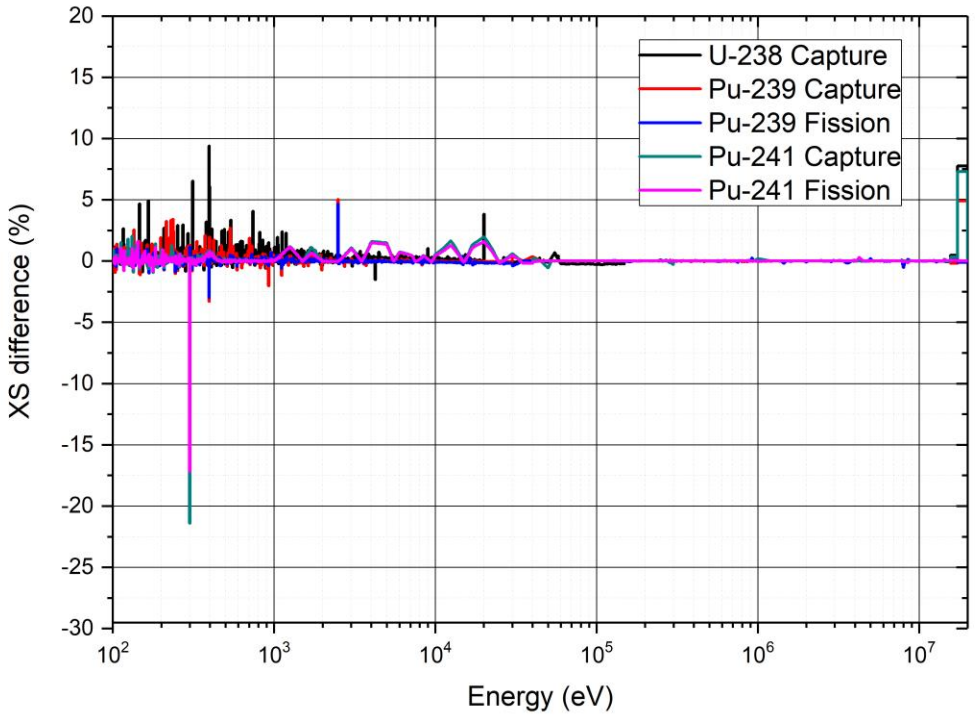

Figure 5.1.5. Cross section differences of U^{238}, Pu^{239}, and Pu^{241} between MG-KENO and MCNP for the MSR problem.

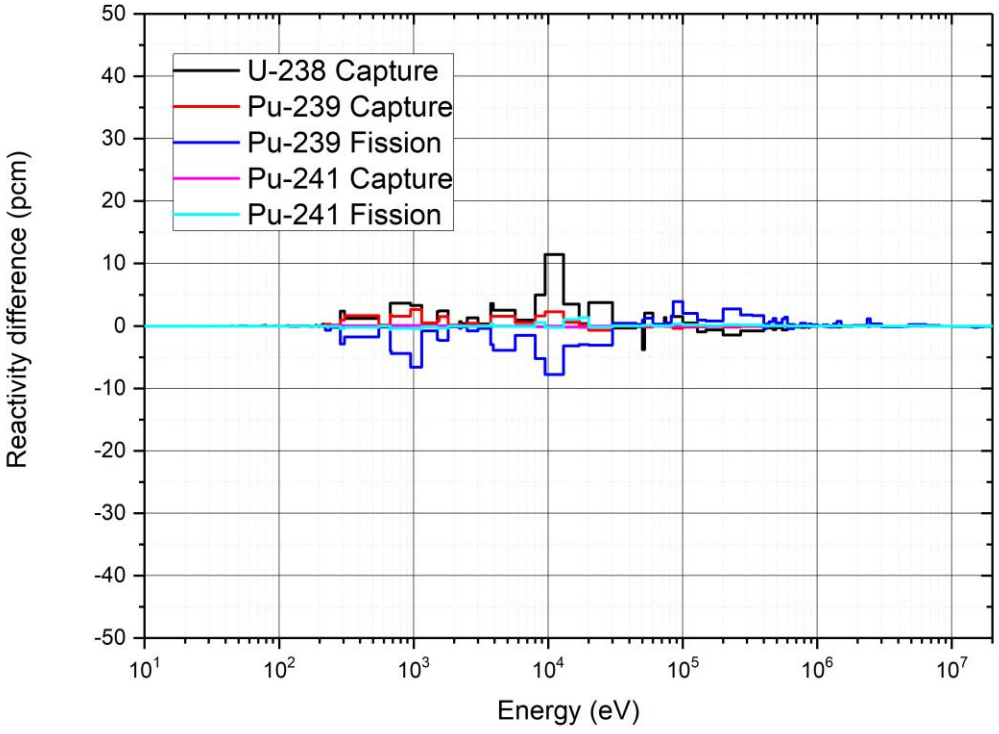

Figure 5.1.6. Reactivity differences due to the cross section and flux differences of U^{238}, Pu^{239}, and Pu^{241} for the MSR problem.

5.2 TWO-STEP UFG LATTICE CALCULATION

It was found that the new UFG AMPX cross section library noticeably enhances the accuracy of the AMPX/SCALE code packages for fast-spectrum applications. However, the UFG lattice calculation is extremely inefficient for practical design calculations. To reduce the computational time to a level similar to the current 252-group lattice calculation without loss of accuracy, a two-step UFG lattice calculation is proposed here. Since the local heterogeneity effects are insignificant in fast reactor problems because of the long neutron mean free path, the UFG slowing-down calculation to determine the detailed neutron spectra could be performed for the corresponding homogeneous medium. Therefore, performing the lattice calculation for a given configuration in two steps using the UFG AMPX library is proposed. In the first step, a UFG slowing-down calculation is performed for the corresponding homogenized composition, and UFG cross sections are collapsed into an intermediate group structure (e.g., the current 252-group structure). In the second step, the lattice calculation is performed in the intermediate group level using the condensed group cross sections. This two-step lattice calculation is similar to the multi-step approach used in PWR assembly calculations, where fine-group pin-cell calculations are first performed, and then the assembly calculation is performed in an intermediate group level with the collapsed group cross sections from pin-cell calculations.

A preliminary verification test of the proposed two-step UFG lattice calculation was performed for a BWR assembly problem with 99% void fraction using in-house slowing-down and 2D MOC solvers from the University of Michigan. The BWR test problem is a 9 × 9 BWR fuel assembly design based on Reference [Aki02], which has five different types of fuel rods with different U^{235} enrichments from 3.0 wt. % to 6.3 wt. %. The isotopic compositions and geometrical configuration of this BWR fuel assembly are presented in Table 5.2.1 and Figure 5.2.1, respectively. Detailed geometric specifications of UO_2 fuel pins can be found in Reference [Aki02]. Note that the two large water rods in the assembly center were represented as seven small water rods with the same volume fractions, and the assembly box and water gaps between assemblies were not modeled for simplicity.

Table 5.2.1 Isotopic compositions of BWR fuel assembly with 99% void fraction

Type	Fuel 1	Fuel 2	Fuel 3	Fuel 4	Fuel Gd	Moderator /Water Rod	
Temp	900K					600K	
Nuclide	Number density					Nuclide	Num.density
U^{235}	1.432E-03	1.137E-03	9.094E-04	6.820E-04	1.039E-03	H^{1}	4.932E-04
U^{238}	2.103E-02	2.132E-02	2.155E-02	2.177E-02	1.949E-03	O^{16}	2.466E-04
O^{16}	4.493E-02	4.492E-02	4.492E-02	4.491E-02	4.399E-03	Zr-nat	4.311E-02
Zr-nat	4.311E-02	4.311E-02	4.311E-02	4.311E-02	4.311E-02	—	
Gd^{154}	—				4.186E-05		
Gd^{155}					2.874E-04		
Gd^{156}					3.995E-04		
Gd^{157}					3.060E-04		
Gd^{158}					4.854E-04		
Gd^{160}					4.309E-04		

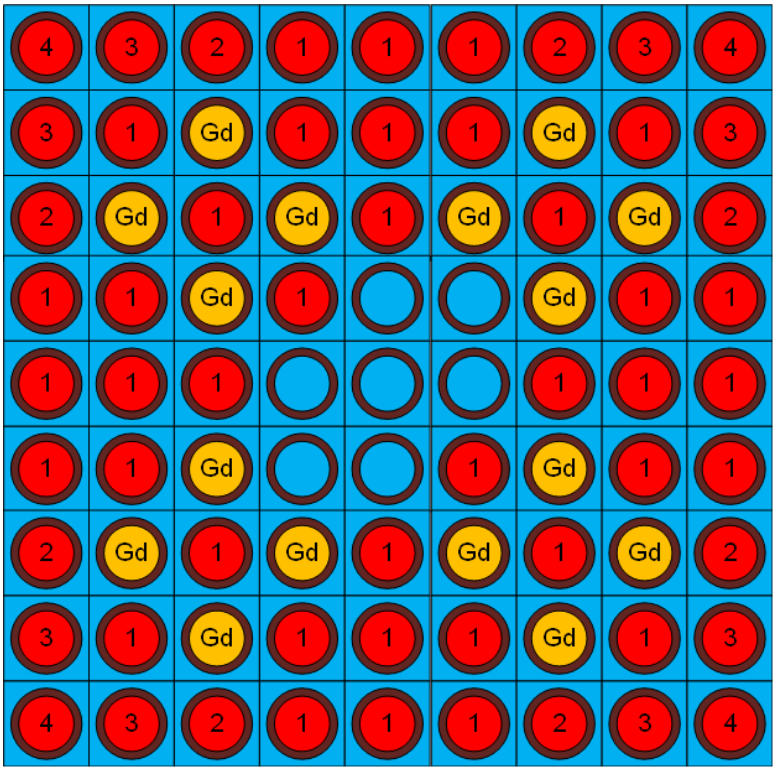

Figure 5.2.1. Geometric configuration of BWR fuel assembly.

A 2,082-group UFG cross section library was obtained from MC^2-3 because of the problems encountered in reading the AMPX 1,585-group working library using the PALEALE module of SCALE, which is summarized in Appendix A. Four different intermediate group structures were tested. The description of intermediate group structures can be found in Reference [Lee11]. The intermediate group cross sections were prepared from a 2,082-group slowing-down calculation for the homogenized assembly composition. The 2D MOC calculation in each intermediate group structure was performed with a ray spacing of 0.05 cm, 16 azimuthal angles, 4 polar angles (for $\pi/2$), and P_2 anisotropic scattering treatment. For comparison, a UFG lattice calculation without the intermediate step was also performed. The reference solution was obtained from a CE MCNP calculation.

Table 5.2.2 compares the eigenvalues obtained from the MCNP and 2D MOC calculations for the four intermediate group structures. This table shows that the 2,082-group MOC solution agrees well with the reference MCNP solution. Furthermore, all the four eigenvalues obtained from the two-step lattice calculations agree well with the UFG solution without the intermediate step. In fact, the two-step results agree slightly better with the MCNP result than the UFG solution because of error cancelation. These results indicate that the UFG spectrum in a fast-spectrum lattice can be well approximated by the UFG spectrum in the corresponding homogenized composition.

Table 5.2.2. Comparison of eigenvalues of BWR fuel assembly with 99% void fraction obtained from two-step lattice calculation

Fuel	Void	k-infinity					
		MCNP	2D MOC (UFG)	Diff (pcm)	2D MOC (intermediate group)		
					Group[a]	k_{inf}	Diff (pcm)
BWR	99%	0.77279 (14)	0.77444	165	425	0.77425	146
					230	0.77424	145
					116	0.77421	142
					33	0.77422	143

[a] Intermediate group library condensed from the 2,082-group library

The preliminary test results with a highly voided BWR assembly problem suggest that the proposed two-step lattice calculation approach is a promising option to enhance the applicability of the AMPX/SCALE system to fast system analysis without a noticeable increase in computational time. However, the optimum number of intermediate groups may depend on the local heterogeneity effect in each problem. Thus, further investigation is required to determine the optimum intermediate group structure for various fast-spectrum problems.

6 CONCLUSION

The AMPX/SCALE MG procedure generates effective neutron cross sections and scattering matrices by using the Bondarenko approach with the AMPX MG library and performing the PW slowing-down calculations. This procedure has been successfully applied to thermal spectrum reactor analysis, but it has limited applicability to fast-spectrum systems such as highly voided BWR assemblies and fast reactor fuels. To identify the major problems of the AMPX/SCALE procedure in generating fast-spectrum cross sections and devise ways to improve the accuracy, various benchmark problems were analyzed using the AMPX 252-group libraries. Detailed reaction rate analyses were performed by determining isotopic reaction rates using MG-KENO calculations and comparing them with MCNP calculation results.

This reaction rate analysis indicated that the observed discrepancies in fast-spectrum cross sections and scattering matrices mainly originate from the limitation of the Bondarenko approach for the 252-group structure. This limitation is caused by the lack of 1/E asymptotic spectrum, strong interactions of multiple resonant nuclides, and broad resonances of intermediate-weight nuclides. In fast-spectrum systems, the broad scattering resonances of intermediate-weight nuclides contributes to the strongly jagged structure of the neutron spectrum, and the asymptotic spectra used in generating the 252-group AMPX library are not attained. A normalization problem in the probabilities tables was also identified and corrected. In addition, a large reactivity error was introduced in the MSR problem by the unshielded (n,p) cross section of Cl^{35}.

To eliminate the limitation of the Bondarenko approach in the 252-group level, adopting a UFG structure was proposed so that the broad scattering resonances of intermediate-weight nuclides can be accurately represented by a piecewise constant function. A UFG AMPX library was genearted in a 1,585-group structure using the AMPX/SCALE code packages and tested against the MCNP calculations. It was found that the new 1,585-group AMPX library resulted in remarkable improvements in 252-group cross sections and reactivity for fast reactor problems. For example, the reactivity error due to U^{238} capture reaction error was reduced from 543 to 53 pcm for the highly voided BWR problem and from 485 to 51 pcm for the MSR problem.

To reduce the computational time of the UFG lattice calculation similar to the current 252-group lattice calculation without loss of accuracy, a two-step UFG lattice calculation was proposed. A preliminary test with a highly voided BWR assembly problem indicated that the proposed two-step lattice calculation approach is a promising option to enhance the applicability of the AMPX/SCALE system to fast system analysis without a noticeable increase in computational time.

REFERENCES

[Aki02] A. Yamamoto, T. Ikehara, et al., "Benchmark Problem Suite for Reactor Physics Study of LWR Next Generation Fuels," vol. 39, no. 8, pp. 900–912 (2002).

[CAS15] "Consortium for Advanced Simulation of Light Water Reactors (CASL)." URL http://www.casl.gov/ (2015).

[Cha06] Y. I. Chang, P. J. Finck, et al., "Advanced Burner Test Reactor Preconceptual Design Report," ANL-ABR-1, Argonne National Laboratory (2006).

[Cse12] Cross Section Evaluation Working Group, "ENDF-6 Formats Manual, Data Formats and Procedures for the Evaluated Nuclear Data File ENDF/B-VI and ENDF/B-VII," CSEWG Document ENDF-102, National Nuclear Data Center, Brookhaven National Laboratory (2012).

[Kim15] K. S. Kim, "Procedure to Generate the MPACT Multigroup Library, Rev. 0," CASL-X-2015-1013-000, Oak Ridge National Laboratory (2015).

[Kim16] K. S. Kim, "Generation of the V4.2m5 AMPX and MPACT 51 and 252-Group Libraries with ENDF/B-VII.0 and VII.1, Rev. 0," CASL-U-2016-1177-000, Oak Ridge National Laboratory (2016).

[Kim17] K. S. Kim, K. Clarno, et al., "Development of the V4.2m5 and V5.0m0 Multigroup Cross Section Libraries for MPACT for PWR and BWR, Rev. 0," ORNL/TM-2017/95, Oak Ridge National Laboratory (2017).

[Lee11] C. H. Lee and W. S. Yang, "MC2-3: Multigroup Cross Section Generation Code for Fast Reactor Analysis," ANL-NE-11-41, Argonne National Laboratory (2011).

[Mpa13] MPACT: User's Manual Version 1.0.0, November 8, 2013.

[Sca16] "SCALE: A Modular Code System for Performing Standardized Computer Analyses for Licensing Evaluation," ORNL-TM/2005/39, Version 6.2, Oak Ridge National Laboratory (2016). (Available from Radiation Safety Information Computational Center at Oak Ridge National Laboratory as CCC-834.)

[Shi12] H. J. Shim, et al., "McCARD: Monte Carlo Code for Advanced Reactor Design and Analysis," *Nucl. Eng. Technol.*, 44, 2, 161 (2012).

[Tau80] M. Taube and W. Heer., "Reactor with Very Low Fission Product Inventory," EIR-Bericht Nr. 411, Swiss Federal Institute of Reactor Technology (1980).

[Tur16] J. Turner, et al., "The Virtual Environment for Reactor Applications (VERA): Design and architecture," *Journal of Computational Physics*, 326, 544 (2016).

[Wia16] D. Wiarda et al., "AMPX-6: A Modular Code System for Processing ENDF/B," ORNL/TM-2016/43, Oak Ridge National Laboratory (2016).

[Wil12] M. L. Williams and K. S. Kim, "The Embedded Self-Shielding Method," PHYSOR 2012, Knoxville, Tennessee, USA, April 15–20, 2012.

[Yan11] W. S. Yang, "Fast Reactor Physics and Computational Methods," *Nucl. Eng. Technol.*, 44, 2, 177 (2011).

APPENDIX A. ERRORS ENCOUNTERED IN PALEALE MODULE

To test the two-step ultra-fine group lattice calculation approach, reading the multi-group cross sections from an AMPX working library using the PALEALE module was attempted. However, incorrect higher order (>P0) scattering matrices were encountered in the PALEALE output for the following benchmark problems:

1) In 252-group scattering matrices, there are elements below the lower limit of the group structure. For example, there are scattering matrix elements from group 253 to 271, when the 252-group AMPX working library was used to list the multi-group cross sections.
2) In the higher order scattering matrices, the within-group scattering cross sections are always larger than the total cross sections.

It should be noted that the principal cross sections and the P0 scattering matrix elements above the lower limit of group structure are reasonable compared to the tallied values of Monte Carlo calculations.